



January 2021

Evaluation Of The Performance Of A Rosemount Icing Detector During Impacts 2020

Greg Lee Sova

[How does access to this work benefit you? Let us know!](#)

Follow this and additional works at: <https://commons.und.edu/theses>

Recommended Citation

Sova, Greg Lee, "Evaluation Of The Performance Of A Rosemount Icing Detector During Impacts 2020" (2021). *Theses and Dissertations*. 4194.
<https://commons.und.edu/theses/4194>

This Thesis is brought to you for free and open access by the Theses, Dissertations, and Senior Projects at UND Scholarly Commons. It has been accepted for inclusion in Theses and Dissertations by an authorized administrator of UND Scholarly Commons. For more information, please contact und.common@library.und.edu.

EVALUATION OF THE PERFORMANCE OF A ROSEMOUNT ICING DETECTOR
DURING IMPACTS 2020

by

Greg Lee Sova

Bachelor of Science, University of Louisiana at Monroe, 2019

A Thesis

Submitted to the Graduate Faculty

of the

University of North Dakota

in partial fulfillment of the requirements

for the degree of

Master of Science

Grand Forks, North Dakota

December 2021

Copyright 2021 Greg Lee Sova

Name: Greg Sova

Degree: Master of Science

This document, submitted in partial fulfillment of the requirements for the degree from the University of North Dakota, has been read by the Faculty Advisory Committee under whom the work has been done and is hereby approved.

DocuSigned by:
David Delene
A58FCE91339F48C

David Delene

DocuSigned by:
Michael Poellot
7A5B4FC10E1D412

Michael Poellot

DocuSigned by:
Andy Detwiler
D67C4766255483

Andrew Detwiler

This document is being submitted by the appointed advisory committee as having met all the requirements of the School of Graduate Studies at the University of North Dakota and is hereby approved.

DocuSigned by:
Chris Nelson
2254F05B2C72623

Chris Nelson
Dean of the School of Graduate Studies

12/9/2021

Date

PERMISSION

| | |
|------------|--|
| Title | Evaluation of the Performance of a Rosemount Icing Detector During IMPACTS 2020 |
| Department | Atmospheric Science |
| Degree | Master of Science |

In presenting this thesis in partial fulfillment of the requirements for a graduate degree from the University of North Dakota, I agree that the library of this University shall make it freely available for inspection. I further agree that permission for extensive copying for scholarly purposes may be granted by the professor who supervised my thesis work, or, in his absence, by the Chairperson of the department or the dean of the School of Graduate Studies. It is understood that any copying or publication or other use of this thesis or part thereof for financial gain shall not be allowed without my written permission. It is also understood that due recognition shall be given to me and to the University of North Dakota in any scholarly use which may be made of any material in my thesis.

Greg Lee Sova

6 December 2021

TABLE OF CONTENTS

| | | |
|--|-----|----|
| LIST OF FIGURES..... | vii | |
| LIST OF TABLES..... | ix | |
| ACKNOWLEDGEMENTS..... | x | |
| ABSTRACT..... | xi | |
| CHAPTER 1 | | |
| INTRODUCTION..... | 1 | |
| 1. Motivation | | |
| 2. Liquid Water Content Probes..... | 3 | |
| 3. Rosemount Icing Detector..... | 6 | |
| 4. Objectives..... | 14 | |
| CHAPTER 2 | | |
| DATA..... | 16 | |
| 1. Field Project Overview..... | | 16 |
| 2. In situ Sampling Aircraft Overview..... | | 17 |
| 3. Data Post-Processing Overview..... | | 19 |
| 4. Flights..... | | 20 |
| CHAPTER 3 | | |
| METHODOLOGY..... | 22 | |
| 1. Supercooled Liquid Water Content Calculation..... | | 22 |
| 2. Analysis..... | | 32 |
| CHAPTER 4 | | |
| RESULTS..... | 39 | |
| 1. SLWC Derivation..... | | 39 |
| 2. Environmental Tests Overview..... | | 41 |

| | |
|---|----|
| 3. Temperature..... | 42 |
| 4. Pitch Angle and Roll Angle..... | 44 |
| 5. True Air Speed..... | 49 |
| 6. Total Particle Concentration and Mean Volume Diameter..... | 54 |
| 7. Minimum Detection Threshold..... | 59 |
| CHAPTER 5 | |
| DISCUSSION AND CONCLUSIONS..... | 61 |
| 1. Discussion..... | 61 |
| 2. Conclusions..... | 63 |
| REFERENCES..... | 66 |
| APPENDIX A | |
| SCRIPTS..... | 71 |

LIST OF FIGURES

| | |
|--|----|
| Figure 1: The Rosemount Icing Detector model 0871ND4-FT..... | 8 |
| Figure 2: Four images from wind tunnel tests of a 871 model Rosemount Icing Detector..... | 9 |
| Figure 3: Graph of the difference between the calculated adiabatic temperature of the Rosemount Icing Detector and the air temperature..... | 11 |
| Figure 4: Instrument configuration of the UND Cloud Probes during IMPACTS 2020..... | 18 |
| Figure 5: Liquid water content from the King Probe and Cloud Droplet Probe and the Rosemount Icing Detector frequency on 1/25/2020 from 22:19:38Z to 22:20:20Z..... | 23 |
| Figure 6: Liquid water content of the King Probe and Cloud Droplet Probe and Rosemount Icing Detector frequency on 2/6/2020 from 00:51:30Z to 00:52:06Z..... | 24 |
| Figure 7: Two Dimensional Stereo Probe images on the 1/25/2020 flight at 22:39Z | 25 |
| Figure 8: Three second averaged liquid water content from the Cloud Droplet Probe and negative change in Rosemount Icing Detector frequency divided by the true air speed on 2/5/2020 from 19:46:34Z to 19:47:36Z..... | 27 |
| Figure 9: Same as Fig. 8 but from 22:54:07Z to 22:56:16Z..... | 28 |
| Figure 10: Rosemount Icing Detector frequency and liquid water content from the King Probe and Cloud Droplet Probe at 2/7/2020 from 19:46:31Z to 19:47:36Z..... | 29 |
| Figure 11: King Probe liquid water content before and after two second averaging at 1/25/2020 from 22:19:38Z to 22:20:20Z..... | 31 |

Figure 12: Merged particle size distribution spectrum from the Cloud Droplet Probe, Two Dimensional Stereo Probe, and High Volume Precipitation Spectrometer Version 3.....36

Figure 13: Two Dimensional Stereo Probe imagery at 2/5/2020 23:46Z.....37

Figure 14: High Volume Precipitation Spectrometer imagery at 2/5/2020 23:46Z.37

Figure 15: Scatterplot of all 8 cases comparing the King Probe liquid water content to the Rosemount Icing Detector change in frequency divided by the true air speed and the probe diameter and length (c).....40

Figure 16: Same as Fig. 15 but with the Cloud Droplet Probe instead of the King Probe.....41

Figure 17: Scatterplots of the Rosemount Icing Detector supercooled liquid water content and Cloud Droplet Probe liquid water content over the four flights in IMPACTS 2020 in which both probes had valid data. From top left clockwise: 12 °C and below, 0 °C and below, -10 °C and below, and -3 °C and below.....43

Figure 18: Plot of the correlation coefficient of various temperature thresholds and the fraction of the total dataset that each threshold represents.....44

Figure 19: Scatterplots of the Rosemount Icing Detector supercooled liquid water and Cloud Droplet Probe liquid water content over the four flights in IMPACTS 2020 in which both probes had valid data. From top left clockwise: all pitch angles, -2° to 2°, 2° and above, and -2° and below.....45

Figure 20: Histogram of the pitch angles over the course of the 1/25/2020 flight. 46

Figure 21: Scatterplot of Rosemount Icing Detector supercooled liquid water content and Cloud Droplet Probe liquid water content over the four flights with valid data from both probes, limited to pitch angles of 3° and above (top), and 3° and below (bottom).....47

Figure 22: Scatterplots of the Rosemount Icing Detector supercooled liquid water content and Cloud Droplet Probe liquid water content over the four flights in IMPACTS 2020 in which both probes had valid data. From top left clockwise: all roll angles, -2° to 2°, 2° and above, and -2° and below.....48

Figure 23: Histogram of roll angles throughout the course of the 2/7/2020 flight. 49

Figure 24: Scatterplot of Rosemount Icing Detector supercooled liquid water content and Cloud Droplet Probe liquid water content scatterplot in the range of -5 °C to -3 °C.....50

Figure 25: Same as Fig. 24, but with a maximum true air speed threshold of 150 m s⁻¹ applied.....51

Figure 26: Histogram of true airspeed throughout the 1/25/2020 flight.....52

Figure 27: Same as Fig. 24, but in the temperature range of -3 °C to -2 °C.....53

Figure 28: Same as Fig. 24 but with temperatures below -10 °C.....54

Figure 29: Scatterplots of the Rosemount Icing Detector supercooled liquid water content and Cloud Droplet Probe liquid water content. Concentration limits, from top left, clockwise: no limit, 10⁸ m⁻³ and less, 2×10⁷ m⁻³ and fewer, 10⁸ m⁻³ and greater.....56

Figure 30: RICE Probe frequency (magenta) and air temperature (red) from 22:52Z to 22:58Z during the 2/5/2020 flight.....57

Figure 31: Mean volume diameter (black) and total concentration above 10⁸ m⁻³ (red) from 22:45Z to 22:58Z during the 2/5/2020 flight.....58

Figure 32: Scatterplots of the Rosemount Icing Detector supercooled liquid water content and Cloud Droplet Probe liquid water content. Mean volume diameter limits, from top left, clockwise: no limit, 50 μm to 200 μm, 150 μm to 200 μm, 0 μm to 50 μm.....59

LIST OF TABLES

| | |
|--|----|
| Table 1: Studies regarding the measuring capabilities of the Rosemount Icing Detector (RICE Probe) and the model of RICE Probe used in each study.. | 14 |
| Table 2: Microphysics probes present on the NASA P-3 Orion for the IMPACTS 2020 Field Campaign. Described in the table are, in order, the Cloud Droplet Probe (CDP), Hawkeye Fast Cloud Droplet Probe (FCDP), Hawkeye Cloud Particle Imager (CPI), Particle Habit Imager and Polarization Scanner (PHIPS), Two Dimensional Stereo Probe (2D-S), High Volume Precipitation Spectrometer Version 3 (HVPS-3), King Liquid Water Sensor (King Probe), Nevzorov Liquid Water Content and Total Water Content Probe (Nevzorov Probe), and Rosemount Icing Detector (RICE Probe)..... | 19 |
| Table 3: General characteristics of the first five science flights during the NASA IMPACTS 2020 field campaign, courtesy of the Aircraft Scorecard at impacts.atmos.washington.edu , retrieved 10/28/2021..... | 21 |
| Table 4: Instrument status of various cloud probes during IMPACTS 2020. Red indicates no probe data, yellow indicates intermittent or low quality instrument data, and green indicates nominal instrument data..... | 21 |
| Table 5: General characteristics of the 8 valid cases used for the empirical derivation of the supercooled liquid water product..... | 26 |

ACKNOWLEDGEMENTS

I would like to first acknowledge my beautiful and loving wife Allison, who is my entire motivation for completion of this degree. I would also like to thank Professor Michael Poellot who gave me the chance to advance my education and work for the University. I would like to thank Dr. David Delene and Dr. Andrew Detwiler, who served on my committee and provided valuable input on both a professional and personal level. Also, Dr. Alexei Korolev and Trece Hopp made separate but significant contributions to my work of which I am thankful. I would like to thank my family, who gave me the life skills and support needed for me to succeed in graduate school. Finally, I would like to thank my friends, of which there would be too many to name, for their contributions. Through a variety of forms of humor and friendship, they were able to help me cope with my surroundings and conditions, even as the coronavirus pandemic changed our way of life drastically right before our eyes.

This work was supported by NASA Grant Number 80NSSC19K0328.

ABSTRACT

The Rosemount Icing Detector (RICE Probe) is a vibrating cylinder icing probe that measures the supercooled liquid water in the atmosphere that contributes to aircraft icing conditions. The frequency of the RICE Probe vibration decreases with increasing ice accretion. The RICE Probe was mounted on the fuselage of the NASA P-3 Orion aircraft for the IMPACTS 2020 field campaign. During the project, flight scientists had real-time frequency data for qualitative assessment of the presence of supercooled liquid water. For quantitative measurements of the liquid water, flight scientists used the King Liquid Water Sensor (King Probe) and the Cloud Droplet Probe (CDP). While the King Probe and CDP perform well in certain conditions, both probes are subject to measurement uncertainties that are dependent on cloud environment.

A supercooled liquid water content (SLWC) product is derived for the model 0871ND4 RICE Probe by comparing the change in output frequency to a known liquid water content measurement in supercooled water-only conditions. The constant relating RICE Probe frequency, true air speed, and the probe dimensions to the SLWC is empirically found to be $4.752 \times 10^{-4} \text{ g Hz}^{-1}$. The SLWC product is then evaluated for different environments to test the effectiveness of the product under a variety of conditions. Temperature is found to be the most important effect, with conditions warmer than $-3 \text{ }^{\circ}\text{C}$ being unsuitable for use. While mounted on the NASA P-3 Orion, pitch angles greater than 3° are found to be unsuitable as

well. At temperatures between $-5\text{ }^{\circ}\text{C}$ and $-3\text{ }^{\circ}\text{C}$, slower air speeds improved the RICE Probe's effectiveness at sampling SLWC.

CHAPTER 1

INTRODUCTION

1. Motivation

In the atmosphere, clouds of hydrometeors may be composed of liquid water droplets, ice crystals, or a mixture of liquid and ice particles that is commonly described as “mixed phase clouds”. The morphology of mixed phase clouds is complex and depends on a variety of variables and factors. The contribution of supercooled water to mixed phase cloud processes has been theorized since the early to mid-20th century and one of the leading theories is the Wegener-Bergeron-Findeisen (hereafter WBF) process (Korolev et al. 2017). At temperatures below $^{\circ}\text{C}$, ice has a lower saturation vapor pressure than water. Water that exists below freezing but has not frozen is considered “supercooled”. When supercooled water droplets and ice crystals coexist in a cloud, the ice grows quicker than the water droplets because the environment is supersaturated with respect to ice. In strong updrafts and areas of isobaric mixing, when the cloud’s vapor pressure is higher than the saturation vapor pressure with respect to both water and ice, both the liquid droplets and ice particles continue to grow. Conversely, when the cloud vapor pressure is less than the saturation vapor pressure with respect to both water and ice, the liquid droplets will evaporate and the ice particles will sublimate. However, when the cloud vapor pressure is greater than the saturation with respect to ice but less than with respect to water, the water droplets evaporate while the ice crystals grow (Korolev 2007). The evaporation of

liquid water adds to the cloud vapor pressure and prolongs the growth of the ice crystals. In the absence of vertical motion, the ice crystals from the supercooled droplet may continue to grow until the droplets have completely evaporated and the cloud reaches saturation with respect to ice. The process of ice growth at the expense of supercooled liquid drops is the WBF process (Stull 2000). Accurately representing the WBF process is of critical importance to weather and climate models, as different treatments of the WBF process can show drastic differences in cloud radiative effect, total water path, and stratiform versus convective precipitation ratio (Storelvmo and Tan 2015). Another process regarding mixed phase cloud morphology is riming, the process of supercooled water freezing on contact with ice crystals. Empirically, the terminal velocity of a particle is related to the diameter of the particle and the diameter is related to the mass of the particle (Rogers and Yau 1989). The fall speed of particles directly affects the water budget for clouds and precipitation in weather and climate models. Therefore, in situ observations of both ice water and liquid water content are important for evaluating and verifying weather and climate models.

The observations of water content are also used in evaluating the accuracy of remote sensing retrievals. For example, recent field campaigns by the National Aeronautics and Space Administration (NASA) including the Midlatitude Continental Convective Clouds Experiment (MC3E), the GPM Cold-Season Precipitation Experiment (GCPEX), the Integrated Precipitation and Hydrology Experiment (IPHEX), the Olympic Mountain Experiment (OLYMPEX), and the Investigation of Microphysics and Precipitation for Atlantic Coast-Threatening Snowstorms (IMPACTS) collected data from in situ aircraft that can be collocated with either ground-based sensors or satellite-based sensors. The objective is to test and improve the current satellite-derived microphysics and precipitation algorithms. These remote sensing measurements help the understanding of cloud

properties, which would lead to direct improvement of operational forecasts and observation of precipitation and clouds (Heymsfield et al. 2017). Additionally, supercooled water has been the focus of field campaigns related to aircraft icing, and studies have targeted particular combinations of supercooled liquid water content, temperature, and drop size for determining specific aircraft icing conditions. Studies of aircraft icing are a direct response to numerous aircraft crashes that have been caused by icing conditions (Bernstein et al. 2019). Considering the applications to aircraft safety, remote sensing, atmospheric modeling, and cloud physics, it is highly important to have accurate in situ measurements of supercooled liquid water content (SLWC).

2. Liquid Water Content Probes

A variety of in situ cloud probes are capable of determining the liquid water content (LWC) in cloud. One such probe is the King Liquid Water Sensor (hereby “King Probe”), formerly known as the CSIRO Liquid Water Probe. The King Probe is a heated copper wire wrapped around a 1.5 mm cylinder which is exposed to the airflow. When water droplets come in contact with the heated wire, the droplets are heated and evaporate. The King Probe is designed to keep the hot wire at a constant temperature, and since the wire loses heat due to droplet heating and evaporation, more power has to be applied in cloud to the wire to maintain the constant wire temperature (King et al. 1978). The equation for the additional power (P) is known, and the equation can be arranged to solve for the liquid water content (w_l):

$$w_l = \frac{P - [C(T_s - T_a)(\rho v)^x]}{l d v [L_v + c_w(T_{sw} - T_a)]}, \quad (1)$$

where l and d are the length and diameter of the cylinder, v is the true air speed (TAS), L_v is the latent heat of vaporization, C and x are calibration constants, T_s is

the temperature of the sensor, T_a is the air temperature, and T_{sw} is the temperature at which water evaporates from the probe, assumed to be 90 °C. The calibration constants are handled in the data processing software and are found by performing out-of-cloud test flights with variations in TAS (Delene et al. 2019).

Unfortunately, the King Probe does not exclusively detect liquid water content in mixed- or ice-phase clouds, as there is some response to ice particles coming into contact with the wire and undergoing phase changes as well. Strapp et al. (1999) found that the “false liquid response” was “on the order of 47%” of the measured ice water content (IWC) by the Nevzorov probe. During one particular case in this study of thunderstorm outflow, the King Probe showed LWC values greater than 0.25 g m^{-3} and the Nevzorov total water content read 0.5 g m^{-3} , but virtually zero signal from a Rosemount Icing Detector, which strongly suggested that the King Probe was in error due to ice contamination. The King Probe also has a drop-size response bias, where the King Probe responds accurately when the mean volume diameter (MVD) is below $40 \text{ }\mu\text{m}$, and above $40 \text{ }\mu\text{m}$ the signal diminishes to the point that at MVD of greater than $100 \text{ }\mu\text{m}$, the probe response requires “substantial correction” (Biter et al. 1987). This is due to the fact that at larger drop sizes, the particles do not have enough time to fully evaporate before being shed from the hot wire. One additional weakness of the King Probe is that when the probe is in-cloud with varying TAS, altitude, or air density, the baseline voltage can drift and erroneous non-zero values for liquid water content can be observed, sometimes necessitating a mid-flight zeroing of the probe when out of cloud (Twohy and Rogers 1993).

Another probe that measures the LWC is the Cloud Droplet Probe (CDP). The CDP is a forward-scattering single-particle counting optical probe, operating by detecting the intensity of forward scattered radiation from a particle that passes through a laser that is exposed to the airflow. The CDP detects light scattered at

angles of 4°-12° from the forward direction of the laser by in-focus particles. Beyond 12°, the light is scattered outside of the window and away from the detector, and with angles shorter than 4°, the reflected light is indistinguishable from the original light emitted from the laser and is directed to the “dump spot monitor” instead of reaching the sizer and qualifier. Particles that are in-focus reflect more light at the qualifier than the sizer and vice versa for out-of-focus particles. The voltage recorded at the sizer is converted to a size based on Mie Theory for in-focus particles (Lance et al. 2010). The CDP measures particle size in 30 bins with a minimum size of 2 μm to a maximum size of 50 μm . By calculating the volume of all of the particles in each size bin, summing the contributions from all bins, and multiplying it by the density of water, a LWC can be defined. At high particle concentrations, the CDP does suffer from an issue called “coincidence”, which is defined as when multiple particles are in the sample volume at the same time. The CDP interprets multiple smaller particles as a single large particle, resulting in an undercounting and oversizing of particles. At particle concentrations of 500 cm^{-3} , the CDP undercounted and oversized in the range of 20-30 percent. Therefore, CDP measurements with the LWC must be used with care; however, multiple methods are available to check for measurement issues that include comparison to other LWC measurements, particle transit time (or pulse durations), and rejected pulses vs accepted pulses (Lance 2012). Similarly to the King Probe, the CDP is sensitive to liquid and ice particles, which can anomalously increase concentrations in mixed phase clouds and can lead to improper sizing because ice crystals do not follow Mie Theory and have a different index of refraction than liquid water. Another issue is the shattering of ice particles on the arm tips of the probe, which would create many small particles; however, anti-shattering tips reduce the problem (Korolev et al. 2017).

3. Rosemount Icing Detector

While various airborne probes are capable of detecting LWC in situ, many such probes (e.g. the King Probe and CDP) suffer from sensitivity to ice crystals and few probes can discriminate between ice and supercooled water. One such probe that does not suffer from anomalous ice influence and can discriminate between non-supercooled and supercooled water is the Rosemount Icing Detector (RICE Probe). The RICE Probe has a nickel alloy vibrating cylinder (40 kHz) measuring 2.54 cm long and 0.635 cm in diameter that is exposed to airflow (Fig. 1). Supercooled water freezes on contact with the cylinder, and the added mass reduces the vibrational frequency. The rate of change in frequency over time is proportional to the supercooled liquid water content that is freezing on the probe. It is this basic principle that will be used to derive a SLWC from the RICE Probe frequency output.

If the frequency drops below a certain point set by the user (typically corresponding to approximately 0.5mm of ice accretion), a heater turns on (“trips”) and melts the ice that is in contact with the probe and the remaining ice and meltwater is shed into the airflow (Baumgardner and Rodi 1989). The heater trip point on the RICE Probe for the NASA IMPACTS field campaign, for example, is approximately 39,800 Hz, or 200 Hz below the baseline frequency of 40,000 Hz. The heater stays on for seven seconds and due to the time it takes for the probe returning to thermal equilibrium with the environment, the signal is unusable for the duration of the heating cycle and several seconds afterwards (Brown 1981). As the return to thermal equilibrium is dependent on a variety of factors including temperature and LWC, the sensor can take anywhere from 9 seconds to 22 seconds after the initial heater trip to return to normal operation. In rare instances with temperatures colder than -18 °C, it might take multiple heating cycles to fully shed the ice, due to insufficient heat being supplied to the surface of

the probe (Cober et al. 2001b). Incomplete deicing is also a problem in particularly low airspeeds or when too much ice is allowed to accrete, as demonstrated in wind tunnel tests shown in Fig. 2. Model calculations and observations show that the coldest supercooled water that the RICE can observe in orographic wave clouds is around $-36\text{ }^{\circ}\text{C}$, below which the concentration and particle sizes of supercooled water droplets were theorized to be too small to be detected by the probe (Heymsfield and Miloshevich 1993).

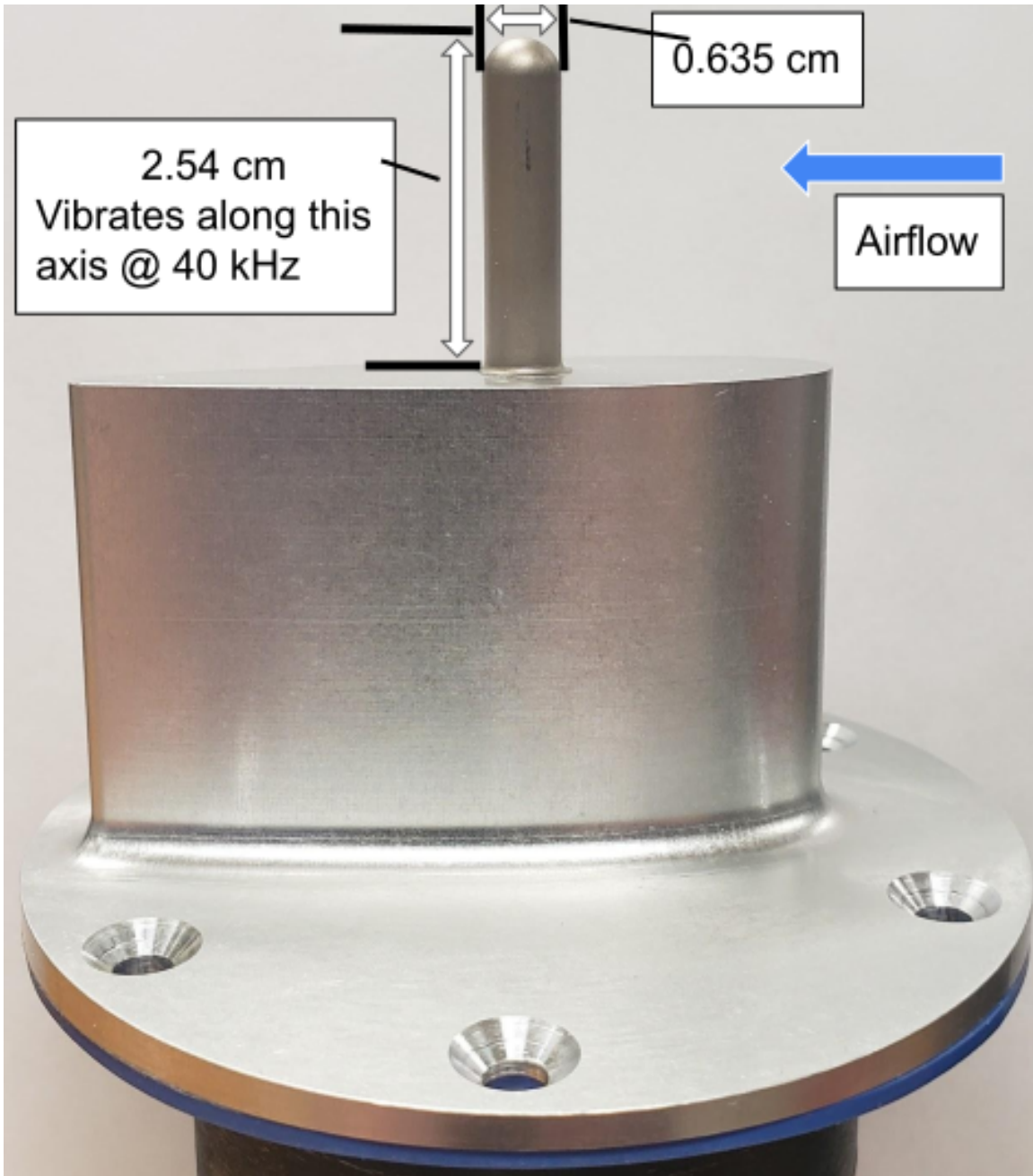


Figure 1: The Rosemount Icing Detector model 0871ND4-FT.

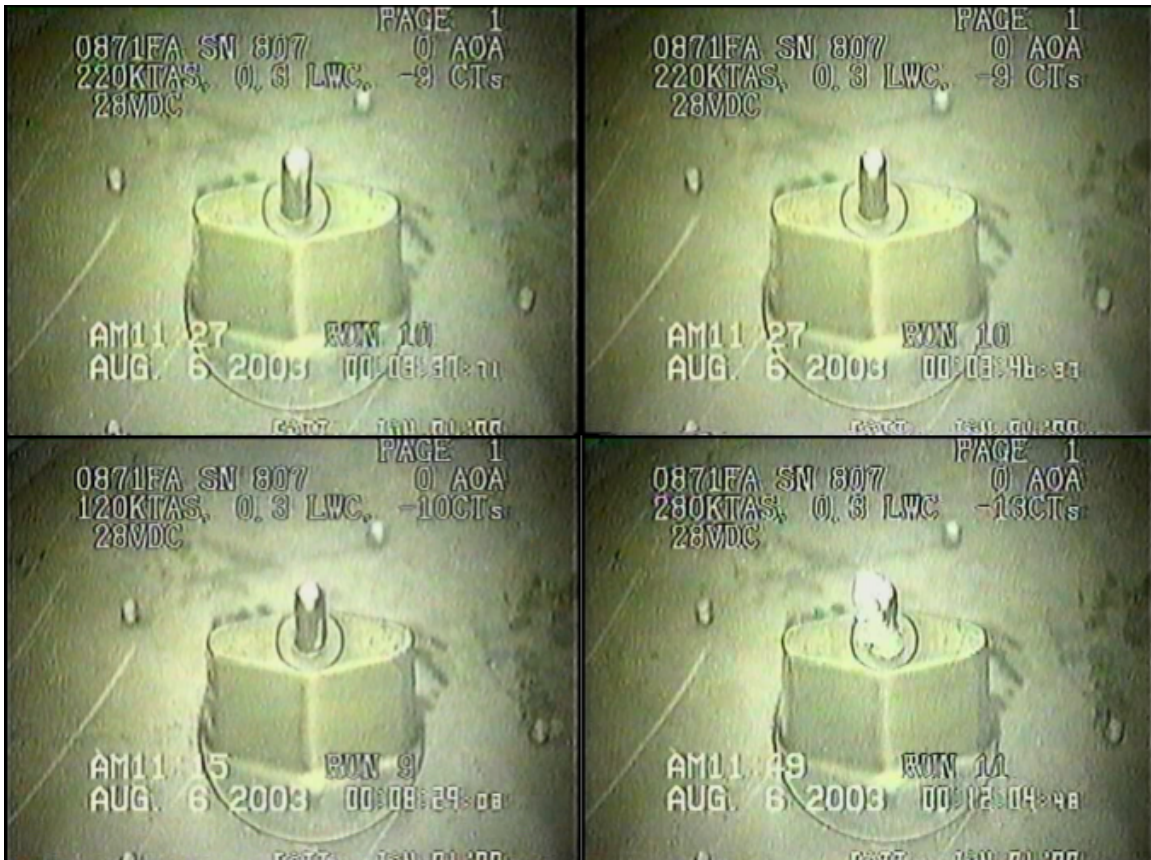


Figure 2: Four images from wind tunnel tests of a 871 model Rosemount Icing Detector. The top left depicts a typical amount of ice accretion before de-icing, while the top right shows the probe clear of ice after a typical de-icing cycle. The bottom left depicts a post-deicing cycle at low airspeeds where the ice has difficulty shedding completely, as ice persists on the right side near the base of the cylinder. The bottom right occurs after more than the standard 0.5 mm of ice has accreted to the probe and an incomplete melting has left some ice on the probe, requiring multiple cycles to completely de-ice. In all pictures, airflow is from right to left. Courtesy of Richard Jeck, FAA Technical Center, 2003.

It is important to note that the design intent of the RICE Probe is not primarily to measure the supercooled liquid water content. The RICE Probe was designed to detect aircraft icing conditions, and while supercooled liquid water is the mechanism behind aircraft icing, not all supercooled liquid water will cause aircraft icing conditions. Particularly, certain processes will cause the surface of the RICE Probe to reach 0 °C even when the ambient air temperature is below 0

°C. These processes govern the Ludlam limit, defined as the critical LWC at which the surface temperature of an object reaches 0 °C, even when the ambient temperature is slightly below 0 °C. The Ludlam limit is governed by multiple thermodynamic processes. One such process is the adiabatic compression of the airflow in front of the probe surface which causes some heating to occur. The compressional heating is shown in Eq. (3) of Mazin et al. (2001):

$$T_{sA} = T_a + \frac{\kappa U^2}{C_p}, \quad (2)$$

where κ , the recovery factor, is assumed to be equal to 0.85, T_{sA} is the adiabatic surface temperature of the probe (°C), T_a is the air temperature (°C), U is the TAS (m s^{-1}), and C_p is the specific heat of air at constant pressure ($\text{J K}^{-1} \text{kg}^{-1}$). The recovery factor accounts for the dissipation of energy due to friction that causes a departure from adiabatic conditions. With a recovery factor of 1, a stream of air impinging on a surface will come to a rest and will completely convert the macroscopic kinetic energy from the air to microscopic thermal motion. This would lead to an ideal adiabatic temperature increase. However, air does not come to a complete rest, leading to a less than ideal adiabatic temperature increase. The magnitude of computed compressional heating over the course of an entire flight is shown in Fig. 3 as the difference between T_{sA} and T_a . Although compressional heating is not the dominant probe warming process, it is not negligible.

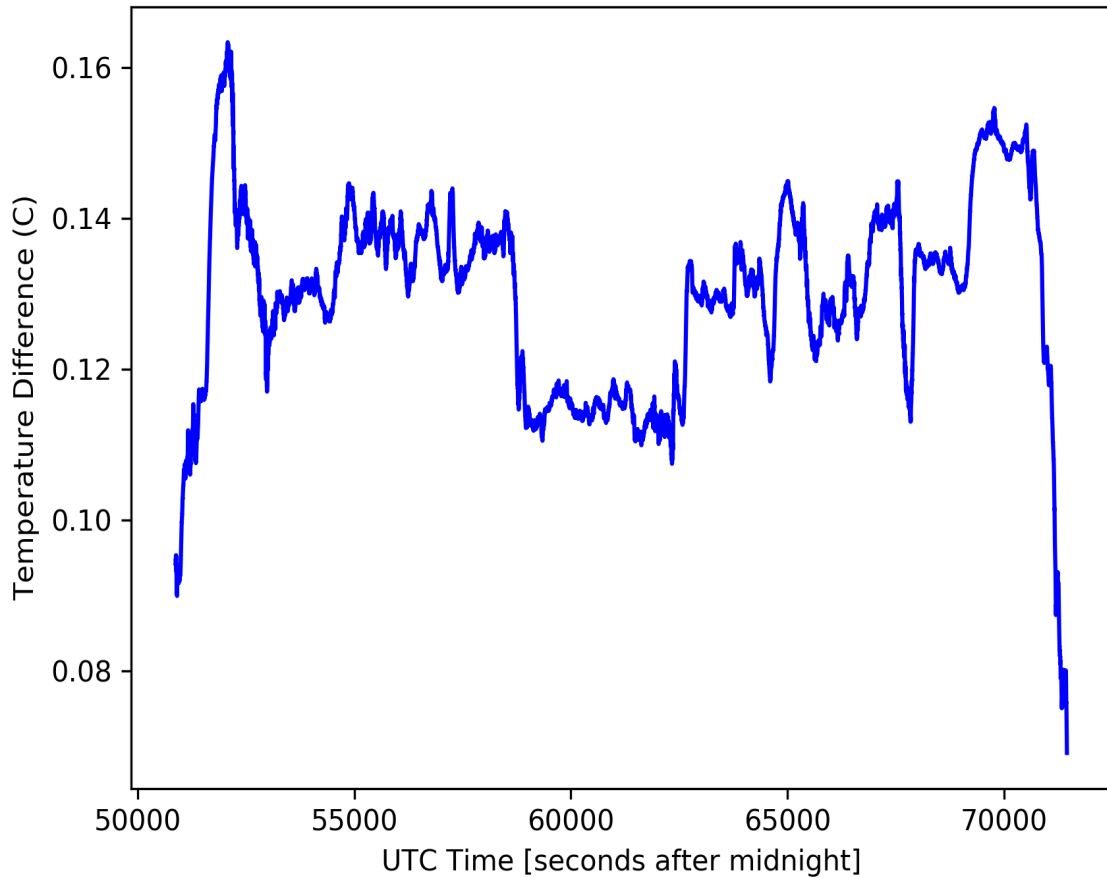


Figure 3: Graph of the difference between the calculated adiabatic temperature of the Rosemount Icing Detector and the air temperature for the 2/7/2020 NASA IMPACTS flight.

The process with the largest influence that causes incomplete freezing of supercooled water onto the surface of the RICE is the release of latent heat of fusion by water freezing on the probe's surface. The process of freezing water onto a surface can be broken down into three steps:

- Supercooled water is heated from its original temperature to 0 °C.
- That water changes phase from liquid to solid, releasing latent heat
- The newly frozen ice is cooled to the sub-0 °C temperature of the RICE Probe

The phase change, in junction with adiabatic compression can raise the temperature of the RICE Probe > 1 °C above the air temperature. When the air temperature is below freezing and close to 0 °C, the RICE Probe temperature can rise above 0 °C, leading to incomplete freezing of supercooled water as some heat has to be transferred from the probe to the supercooled water. Water may be shed into the airflow before it can freeze, leading to the RICE signal underrepresenting the actual SLWC (Fraser et al. 1953). The Ludlam limit is largely dependent on temperature, air speed, and air pressure. As described by Mazin et al. (2001), the Ludlam limit (W_{cr}) is described by the following equation:

$$W_{cr} = \frac{\varphi_0 \alpha}{\varepsilon U} \frac{\frac{\xi R_a L_{is}}{C_p R_v P_a} [E_w(0) - E_w(T_a)] - \frac{\kappa U^2}{2 C_p} - T_a}{L_f + C_w T_a}, \quad (3)$$

where φ_0 is the polar angle above which a particle in the airflow will not make contact with the cylinder, α is the heat transfer coefficient averaged over the whole cylinder, ε is the integral collision efficiency, U is the TAS, ξ is a coefficient dependent on φ_0 , R_a and R_v are the specific gas constants of air and water vapor respectively, L_{is} is the latent heat of evaporation at air temperature T_a , C_p is the specific heat of air at constant pressure, P_a is the air pressure, E_w is the saturation vapor pressure, κ is the recovery factor, L_f is the specific latent heat of water freezing at $T_a = 0$ °C, and C_w is the specific thermal capacity of water. By the Mazin et al. (2001) calculation, for a temperature of -5 °C, air speed of 150 m s⁻¹, and air pressure 850 mb, the critical water content is 0 g m⁻³, meaning the RICE will theoretically not reliably detect any supercooled water at those conditions.

Past field campaigns in icing conditions have used a model of the RICE Probe that works on the principle of recording an analog voltage that is proportional to the frequency of oscillation. Typically, the precision is 1 mV in the range of 0-5 V (Heymsfield and Miloshevich 1989). Another model of the RICE Probe recorded

the number of heater cycles over a given time and related the rate of heater cycles to LWC, though the study acknowledged that the data resolution would be higher with a direct analysis of the probe frequency (Claffey et al. 1995). The RICE Probe used on IMPACTS 2020 is model 0871ND4-FT, which uses a digital output of frequency. The resolution is 1 Hz over an approximate range between 40,000 and 39,800 Hz. The digital frequency model has a coarser resolution than the analog voltage model, but is a finer resolution than the heater cycle count model. Current guidance recommends against using the RICE Probe for quantitative assessments of LWC due to low accuracy (Korolev et al. 2017), though prior to 2021 no known attempts were made to generate a quantitative SLWC product with the digital frequency model of the RICE. Table 1 contains the model number and serial numbers of past RICE probes that have been studied, including the current model used in the IMPACTS 2020 field campaign. Regardless of data measuring technique, the physical properties of the RICE Probe are largely unchanged over decades of use in atmospheric studies, which means the theory of known calibration procedures is still valid and can be applied to the current model with only minor modification.

Table 1: Studies regarding the measuring capabilities of the Rosemount Icing Detector (RICE Probe) and the model of RICE Probe used in each study.

| Author (Year) | RICE Probe Model |
|-----------------------------|-------------------------|
| Sova (2021) | 0871ND4-FT |
| Jeck (2007) | 0871FA |
| Jackson et al. (2003) | 0871 series |
| Cober et al. (2001c) | 871FA221B |
| Isaac et al. (2001) | 871FA |
| Jackson et al. (2001a) | 0871BN3-3 |
| Jackson et al. (2001b) | 0871 series |
| Claffey et al. (1995) | 871CB1, 872B12, 872DC |
| Baumgardner and Rodi (1989) | 871FA |
| Brown (1981) | 871FA212SCI |

4. Objectives

The first objective of this study is to perform an empirical fit of RICE Probe (model 0871ND4-FT) response to LWC measurements to generate a quantitative SLWC product from the RICE Probe. The SLWC product will serve to add to the suite of microphysical products provided to researchers using the RICE Probe in field campaigns. Since 2001, studies that utilize a RICE Probe in a quantitative sense have become exceedingly rare. Recent studies simply utilize the probe as a qualitative assessment of whether supercooled water is present in the atmosphere at a given time (Cober et al. 2001a; Cober and Isaac 2006; Plummer et al. 2014; Borque et al. 2019). The need for quantitative LWC and drop sizes in supercooled

conditions has been highlighted by Isaac et al. (2001), while the measurement and segregation of ice crystals and liquid droplets has been described as “the most complex task” (Korolev et al. 2017).

The second objective is to determine under what conditions the RICE Probe performs well by comparing the RICE Probe to the King Probe and CDP. The RICE Probe SLWC product is compared to the King Probe LWC and CDP LWC data to check for differences that correspond to varying temperatures, air speeds, pitch angles, roll angles, particle size regimes, and particle concentration regimes. Every probe has limitations of what conditions it can perform optimally (or at all), and the RICE Probe is no exception. By identifying these limitations, the effective usage of the probe can be better understood.

CHAPTER 2

DATA

1. Field Project Overview

NASA is tasked with advancing the scientific understanding of the atmosphere and to meet society's needs pertaining to atmospheric events. NASA meets those needs through long-term observation of the atmosphere using satellites and with more limited but in-depth sub-orbital field campaigns. IMPACTS is one such campaign, originally slated to run in the January and February months of 2020-2022, but 2021's Intensive Operational Period (IOP) was delayed to 2023 due to the COVID-19 pandemic. IMPACTS is the first NASA mission to study East Coast snowstorms since the Genesis of Atlantic Lows Experiment (GALE) in 1986 (McMurdie et al. 2020). IMPACTS's focus is on the banded structures of snowstorms that produce heavy snowfall amounts. The goals of IMPACTS are to characterize the spatial and temporal scales of banded features, understand banded structures at the dynamical, thermodynamical, and microphysical level, and apply the understanding of banded structures to improve remote sensing and prediction of Northeast US snowfall. IMPACTS aims to achieve these goals by collecting data from in situ aircraft, ground based instruments, remote sensors on a satellite-simulating high-altitude aircraft, geostationary and polar orbiting satellites, and model simulations. Due to January and February 2020 having fewer than average snowstorms in the primary domain of the Northeast US Atlantic Coast, aircraft

flights were also conducted in the US Midwest region and in the vicinity of the North Carolina coastal region. Every quadrant of a cyclone was sampled at least once, and the stage of cyclone development ranged from incipient to mature, with most observations conducted in the developing phase. Flight profiles consisted of stacked “bowties” and “racetracks” at varying elevations at roughly the same location. A large amount of data was collected for each flight, with some flights consisting of five hours of in situ data per flight.

2. In situ Sampling Aircraft Overview

The observing platform used to collect in situ measurements during IMPACTS was the NASA P-3 Orion aircraft with tail number N426NA (P-3). The P-3 Orion aircraft is a four-engine turboprop aircraft developed by Lockheed that was first built in 1959. Known for its exceptional range and reliability (Boyne 2014), the P-3 Orion is well-suited for long cloud penetrating missions even in icing conditions. The NASA P-3 Orion provides in situ measurements up to 8 km in altitude for up to 14 hours in duration, depending on crew and payload and can be configured for the specific requirement of the project’s research interests (Cropper 2021).

The IMPACTS instrumentation suite includes various cloud probes (Fig. 4, Table 2). Standard atmospheric and geographic variables (e.g. temperature, dew point, latitude, longitude, pressure altitude) are also measured. The computer for acquisition and display of several cloud probe instruments is the Science Engineering Associates (SEA Inc.) model M-300 data acquisition system. The M-300 acquires data from the RICE Probe, CDP, and King Probe, and saves data in a binary formatted file (*.sea) that includes meta-data instrument headers. The Two-Dimensional Stereo (2D-S) Probe and High Volume Precipitation Spectrometer Version 3 (HVPS-3) each have their own data acquisition system, with all system time synced at the start of an aircraft flight.



Figure 4: Instrument configuration of the UND Cloud Probes during IMPACTS 2020. The Rosemount Icing Detector (RICE Probe) is mounted on the fuselage on the starboard side of the forward portion of the aircraft (top left). Probes mounted on wing pylons include a Two-Dimensional Stereo (2D-S) probe (bottom right), two High Volume Precipitation Spectrometer Version 3 (HVPS-3) probes (bottom left), a King Liquid Water Sensor (King Probe), and a Cloud Droplet Probe (CDP), the latter two being mounted on the same boom (top right).

Table 2: Microphysics probes present on the NASA P-3 Orion for the IMPACTS 2020 Field Campaign. Described in the table are, in order, the Cloud Droplet Probe (CDP), Two Dimensional Stereo Probe (2D-S), High Volume Precipitation Spectrometer Version 3 (HVPS-3), King Liquid Water Sensor (King Probe), and Rosemount Icing Detector (RICE Probe).

| Abbreviation | Particle Size Range | Measurement Method |
|---------------------|------------------------------|---------------------------|
| CDP | 2-50 μm | Forward Scattering |
| 2D-S | 10 μm to 6.4 mm | Particle Imaging |
| HVPS-3 | 150 μm to 19.2 mm | Particle Imaging |
| King Probe | 5 to 50 μm | Hot-Wire |
| RICE Probe | Unknown | Vibrating Cylinder |

3. Data Post-Processing Overview

The Airborne Data Processing and Analysis (ADPAA) Software Package (Delene 2011) is used for quality control and assurance in post-processing the files from the M300. ADPAA is open source software designed to automate post-processing of airborne data and for preliminary data files to be made available within hours of a flight. Quick availability post-flight makes it possible for scientists to quality control the data and check instrument status in a timely fashion in case of a quick turnaround between missions. Post-processing occurs at five levels:

- Level 0: The raw data file from the M-300.
- Level 1: The data file for each instrument individually.
- Level 2: The converted analog data into physical measurements, such as a temperature sensor's voltage output converted to $^{\circ}\text{C}$.
- Level 3: Combined derived parameters from multiple probes within the M-300 data stream, such as the King Probe LWC product that is calculated from the King Probe voltage and TAS sensor.

- Level 4: Combined derived parameters from multiple data acquisition systems, such as a combined spectrum of particle size from a CDP, 2D-S, and HVPS-3.

Additionally, a single summary file is compiled from multiple project-specific files. The data obtained in IMPACTS 2020 with the P-3 and processed (Delene et al. 2020) on 28 September 2020 are used. The RICE frequency, King LWC, CDP LWC and mean diameter, aircraft altitude, TAS, pitch angle, roll angle, and air temperature are all relevant to RICE Probe SLWC derivation and analysis and are present in the summary file (*.impacts) from ADPAA at 1 Hz temporal resolution.

4. Flights

The IMPACTS 2020 field campaign featured nine science flights during which the P-3 gathered in situ data. Instrument errors and malfunctions limited the amount of data available for this study, and thus King Probe data are only available for flights 1-5 and the CDP data are only available for flights 2-5. Despite the limitations, the flights sampled in a variety of sampling locations and storm characteristics, as described in Table 3. The full instrument status of the UND Cloud Probes throughout IMPACTS 2020 is shown in Table 4.

Table 3: General characteristics of the first five science flights during the NASA IMPACTS 2020 field campaign, courtesy of the Aircraft Scorecard at impacts.atmos.washington.edu, retrieved 10/28/2021.

| Date | Sampling Location | Development Stage | Sector | Hours |
|-------------|-------------------------------|--------------------------|---------------|--------------|
| 01/18/2020 | New England/New York | Mature | NE | 5 |
| 01/25/2020 | New England/New York | Mature | NE | 5 |
| 02/01/2020 | North Carolina/Virginia Coast | Incipient/Developing | NE | 4 |
| 02/05/2020 | Illinois/Indiana | Developing | NW | 3.5 |
| 02/07/2020 | New England/New York | Rapidly Deepening | NE/NW | 3.5 |

Table 4: Instrument status of various cloud probes during IMPACTS 2020. Red indicates no probe data, yellow indicates intermittent or low quality instrument data, and green indicates nominal instrument data.

| Probe | 1/18 | 1/25 | 2/1 | 2/5 | 2/7 | 2/13 | 2/18 | 2/20 | 2/25 |
|----------|--------|--------|--------|-------|-------|--------|-------|-------|--------|
| 2D-S | Green | Green | Green | Green | Green | Yellow | Green | Green | Yellow |
| CDP | Red | Green | Green | Green | Green | Red | Red | Red | Red |
| HVPS-3A | Green | Green | Green | Green | Green | Green | Green | Green | Green |
| HVPS-3B | Yellow | Yellow | Yellow | Red | Green | Green | Green | Green | Green |
| King | Green | Green | Green | Green | Green | Red | Red | Red | Red |
| Nevzorov | Green | Green | Red | Red | Red | Red | Red | Red | Red |
| RICE | Green | Green | Green | Green | Green | Green | Green | Green | Green |

CHAPTER 3

METHODOLOGY

1. Supercooled Liquid Water Content Calculation

In order to isolate the best cases where the RICE Probe frequency was changing in response to supercooled water, it is desirable to find the periods of time with the most rapid RICE Probe frequency change, indicating the strongest regions of SLWC. Logically, periods of time where the supercooled liquid water accretion was intense enough to trigger a deicing cycle are most desirable to analyze. Each sharp increase of the RICE Probe frequency is noted, as large frequency spikes indicate that the RICE Probe accreted a sufficient amount of ice to warrant a de-icing cycle. Over flights 2-5 (those with LWC products available from both the CDP and King Probe), 60 deicing cycles were found in the RICE Probe data, indicated by sharp increases in frequency from the trip point around 39,800 Hz to 40,000 Hz in a short period of time (typically around 5 seconds). From the 60 deicing cycles indicating high accretion of supercooled water, cases are initially defined as the period starting when the RICE Probe frequency dropped below 40 kHz most recently before the heater cycle and ending 5 seconds prior to the sharp frequency increase that indicates a deicing cycle. A five second buffer is included because visual inspection of the RICE Probe frequency data often showed an anomalous decrease in frequency immediately preceding the sharp increase (Fig. 5). The anomalous frequency decrease would cause any SLWC

product derived from frequency change to be erroneously high. With some icing periods immediately following others, some cases are concatenated (Fig. 6) and the period from 5 seconds prior to increase until the frequency dropped below 40 kHz again between cycles was omitted. The period of time between icing periods is not included because immediately after the de-icing heater turns off, the probe surface is too hot to accumulate ice and must cool down in the airflow to thermal equilibrium. Until thermal equilibrium is met, the RICE will not completely sample the environmental SLW. Concatenation of cases leaves 40 cases to be considered.

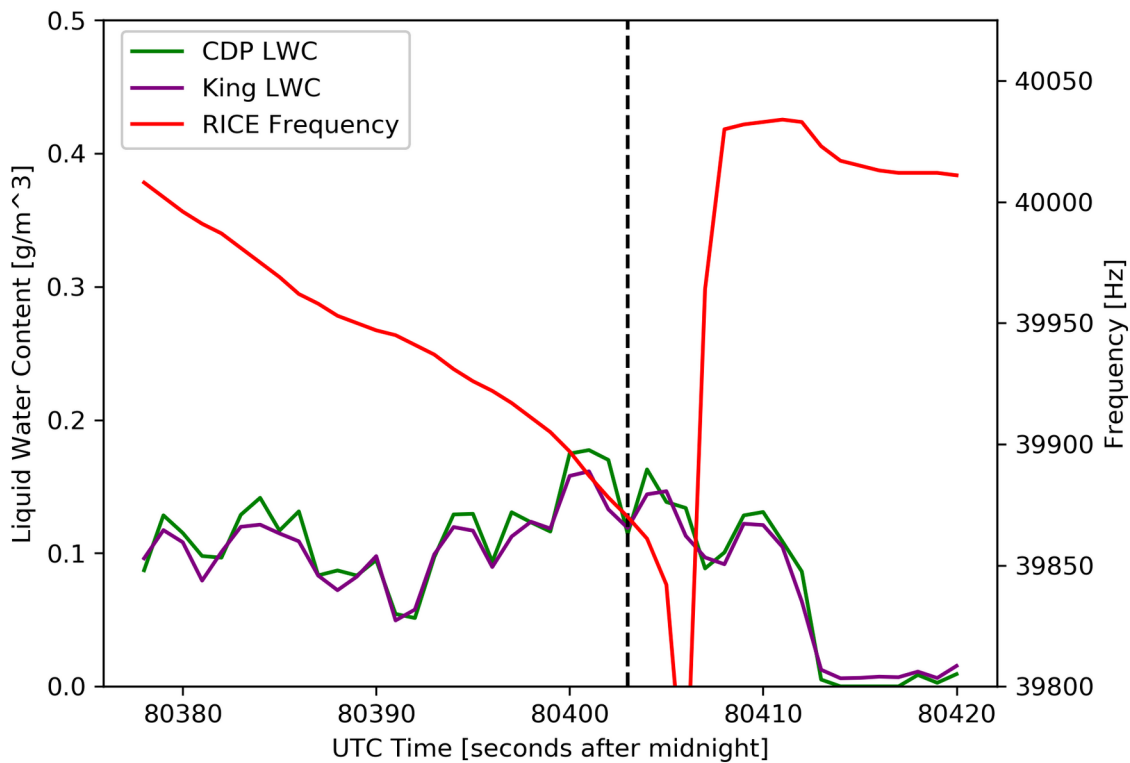


Figure 5: Liquid water content from the King Probe and Cloud Droplet Probe and the Rosemount Icing Detector frequency on 1/25/2020 from 22:19:38Z to 22:20:20Z in a region of a supercooled liquid phase cloud. For case selection purposes, the case here runs from 80380 seconds to 80403 seconds after midnight (vertical dashed line).

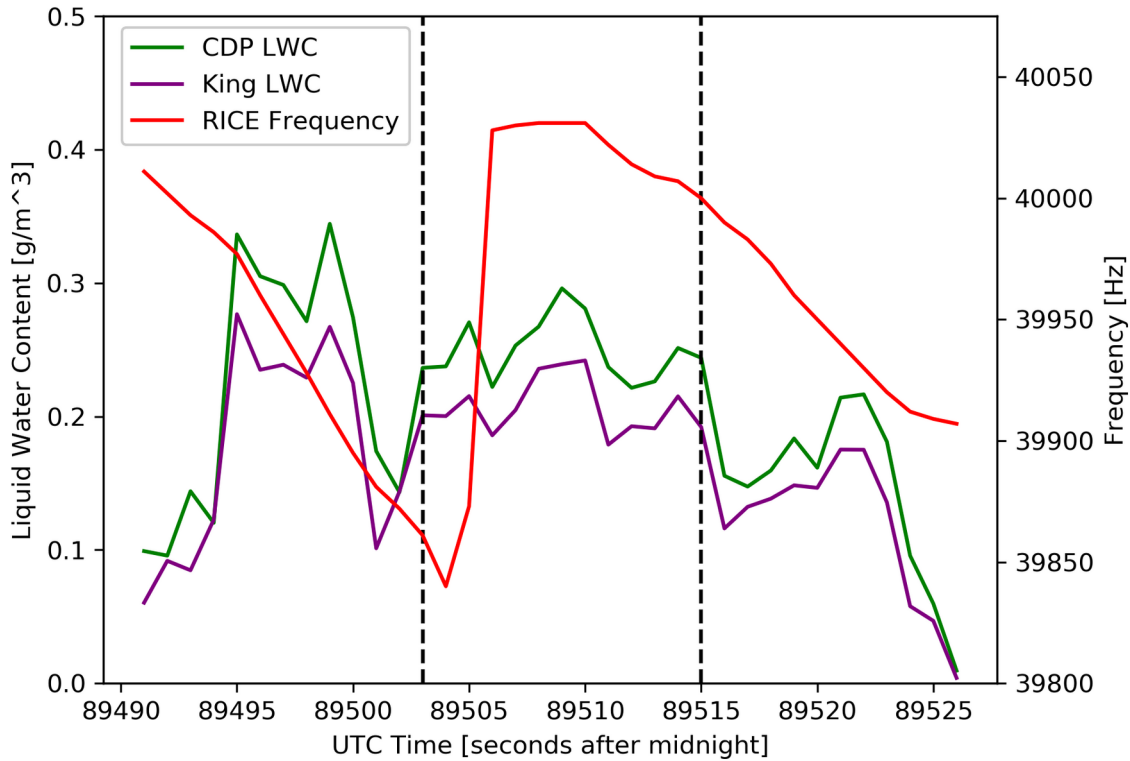


Figure 6: Liquid water content of the King Probe and Cloud Droplet Probe and Rosemount Icing Detector frequency on 2/6/2020 from 00:51:30Z to 00:52:06Z. The case includes all data except what is between the two dashed lines, constituting the heating cycle and return to thermal equilibrium.

Considering the RICE Probe, CDP, and King Probe LWC measurements, the RICE probe is the only instrument that is totally insensitive to ice particles. Therefore, ice particle-free cases need to be selected to compare the RICE Probe’s frequency response to a LWC measurement. The phase is determined to be ice-free when particles on 2D-S images are mostly spherical (Fig. 7) and particles greater than 100 μm as shown on the 2D-S are in concentrations below 10^4 m^{-3} . Additionally, the MVD of the 2D-S must be under 50 μm to account for the CDP’s upper size limit of 50 μm and the King Probe’s gradual reduction in signal with increasing mean volume diameters above 40 μm . Phase discrimination is a significant limit to the number of cases, as mixed phase conditions were quite

common in IMPACTS flights. A phase filter reduces the quantity of cases from 40 to just 9.

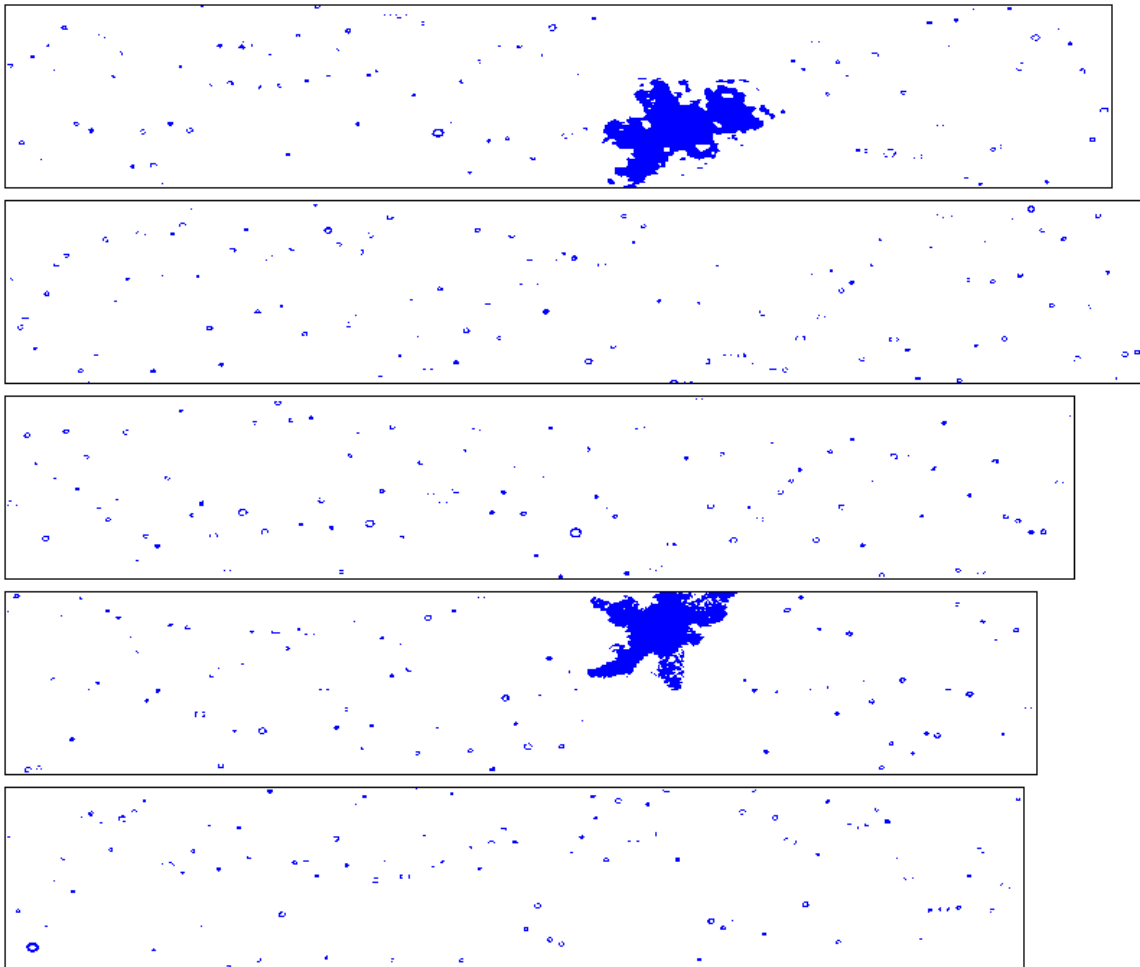


Figure 7: Two Dimensional Stereo Probe images on the 1/25/2020 flight at 22:39Z during a period of icing. Pixel resolution is 10 μm , each strip is 128 pixels tall for a scale of 1,280 μm in the y axis for each strip. Periods of time with no diodes shadowed are omitted.

Finally, a temperature limit has to be considered because at temperatures close to the Ludlam limit, the water would not completely freeze and would be underrepresented on the RICE Probe while the water would still be accurately represented on the CDP or King Probe. Cober et al. (2001b) found that the falloff in signal from Ludlam limit factors occurred mostly in the -2 to -3 $^{\circ}\text{C}$ range,

though that study operated in airspeeds of around 100 m s^{-1} as opposed to typical airspeeds of the P-3 Orion which are around 160 m s^{-1} (Fig. 26). To account for the air speed difference, the temperature threshold for the empirical fit was set to the colder end of the Cober et al. (2001b) range at $-3 \text{ }^{\circ}\text{C}$. Only 1 of the 9 remaining cases was warmer than $-3 \text{ }^{\circ}\text{C}$, leaving 8 final cases for consideration (Table 5). A comparison of the warm case compared to a cold case cases is provided in Fig. 8 and Fig. 9. The warmer case has a much weaker response from the RICE Probe than the colder case and the correlation coefficient from linear regression is also much smaller, with the warmer case having a correlation coefficient of 0.23 compared to 0.94 for the colder case.

Table 5: General characteristics of the 8 valid cases used for the empirical derivation of the supercooled liquid water product.

| Date mm/dd/yyyy | Time Zulu | Max. Temp. $^{\circ}\text{C}$ | Av. 2D-S Conc. >100 μm m^{-3} | Av. 2D-S MVD μm |
|----------------------------------|----------------------------|---|---|--|
| 01/25/2020 | 22:19:38- 22:20:08 | -12.5 | 2,459 | 43.35 |
| 01/25/2020 | 22:39:25- 22:39:51 | -12.2 | 741 | 29.22 |
| 01/25/2020 | 22:43:02- 22:43:33 | -12.8 | 34 | 29.22 |
| 02/05/2020 ^a | 19:46:34- 19:47:36 | -16.5 | 5,457 | 20.59 |
| 02/05/2020 ^a | 20:12:26- 20:13:24 | -16.5 | 203 | 16.80 |
| 02/05/2020 | 21:11:02- 21:12:12 | -11.2 | 334 | 38.25 |
| 02/06/2020 ^b | 00:51:32- 00:52:16 | -8.5 | 1,045 | 29.51 |
| 02/07/2020 ^c | 18:08:35- 18:11:23 | -22.5 | 1,460 | 14.22 |

a: Extensive periods of sublimation omitted

b: Two icing periods

c: Period of missing King Probe data omitted

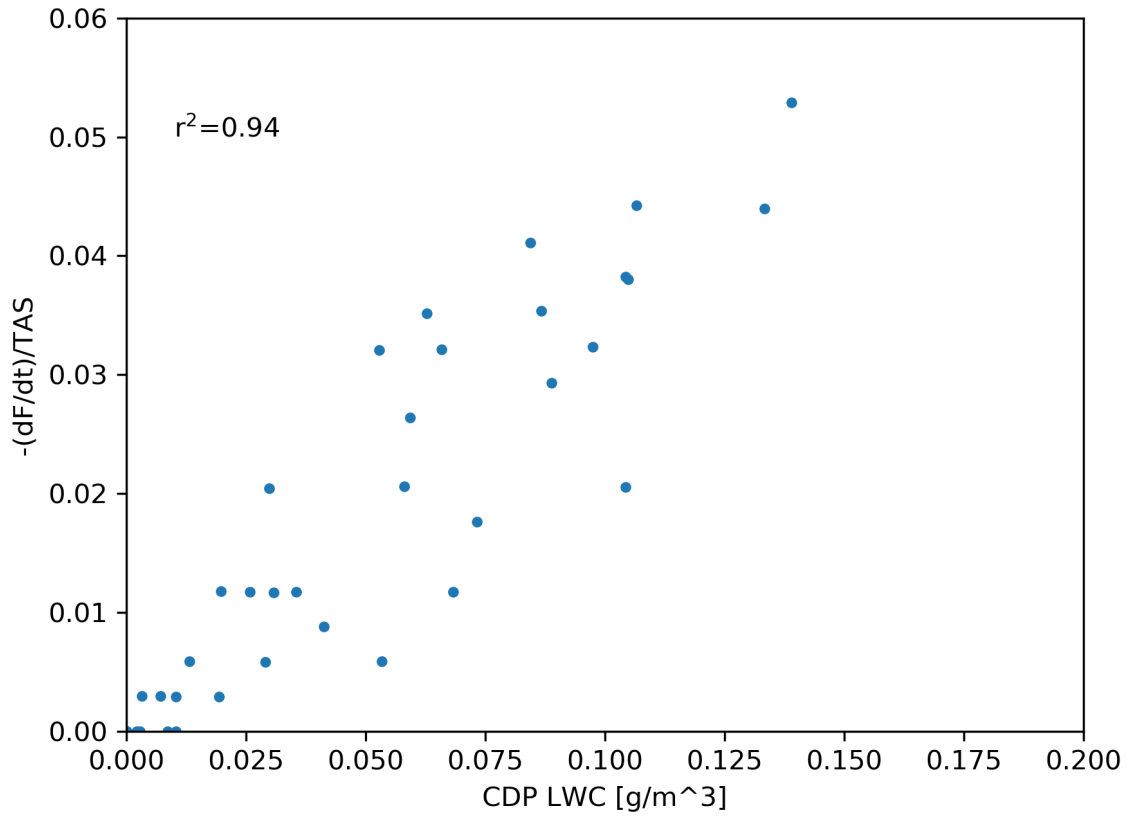


Figure 8: Three second averaged liquid water content from the Cloud Droplet Probe and negative change in Rosemount Icing Detector frequency divided by the true air speed on 2/5/2020 from 19:46:34Z to 19:47:36Z. The maximum temperature in this case was -16.5 °C.

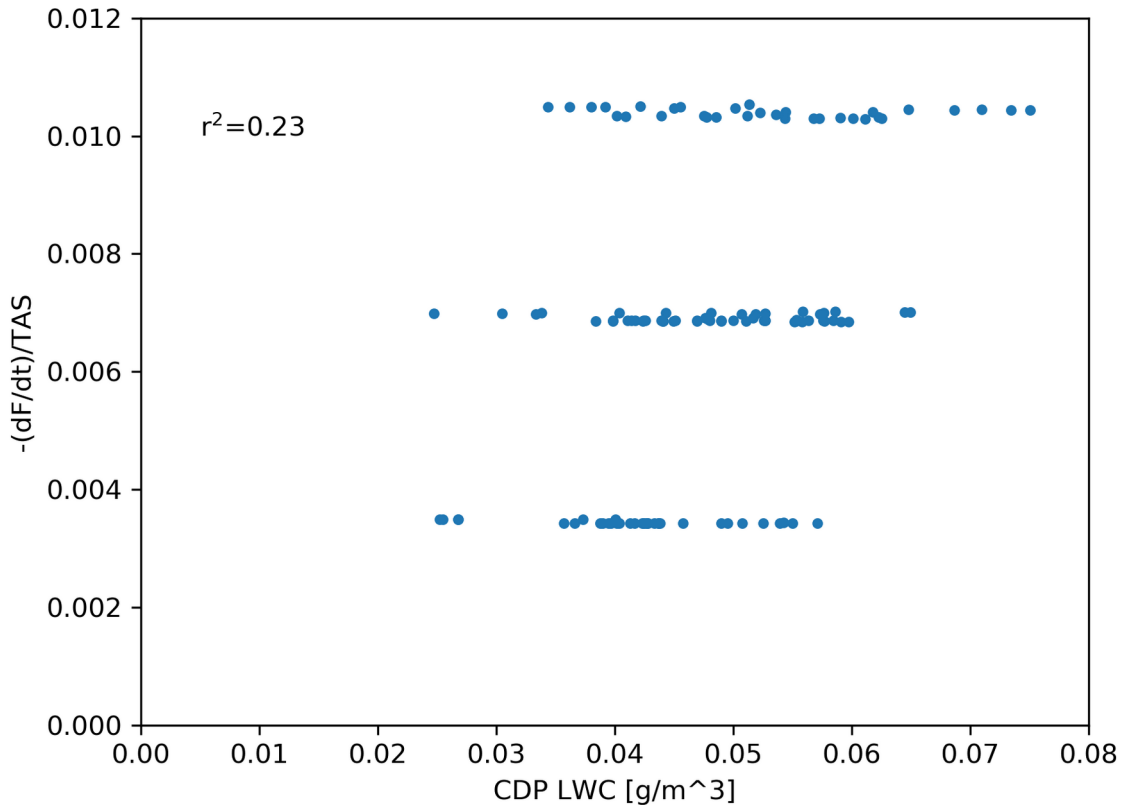


Figure 9: Same as Fig. 8 but from 22:54:07Z to 22:56:16Z. The maximum temperature in this case was -0.8 °C.

For these 8 cases available to generate the SLWC product, additional quality control measures are taken. Times when either the King Probe or CDP LWC values are missing are omitted. Missing data for the King Probe occurred in the 2/7/2020 1811Z case for approximately 129 seconds out of the total of 165 seconds of the cycle. Individual periods of positive RICE Probe frequency change with time are manually removed, as positive frequency change would otherwise indicate that the RICE Probe was not accumulating supercooled water. These instances occur when ice is removed from the RICE Probe, most commonly by sublimation in dry air, such as in Fig. 10. Finally, if there are any major data outliers or data that would indicate a physically impossible condition, those data

points are omitted as well. One such instance of outlier values occurred in the 2/7/2020 1946Z case when the King Probe recorded some negative LWC values.

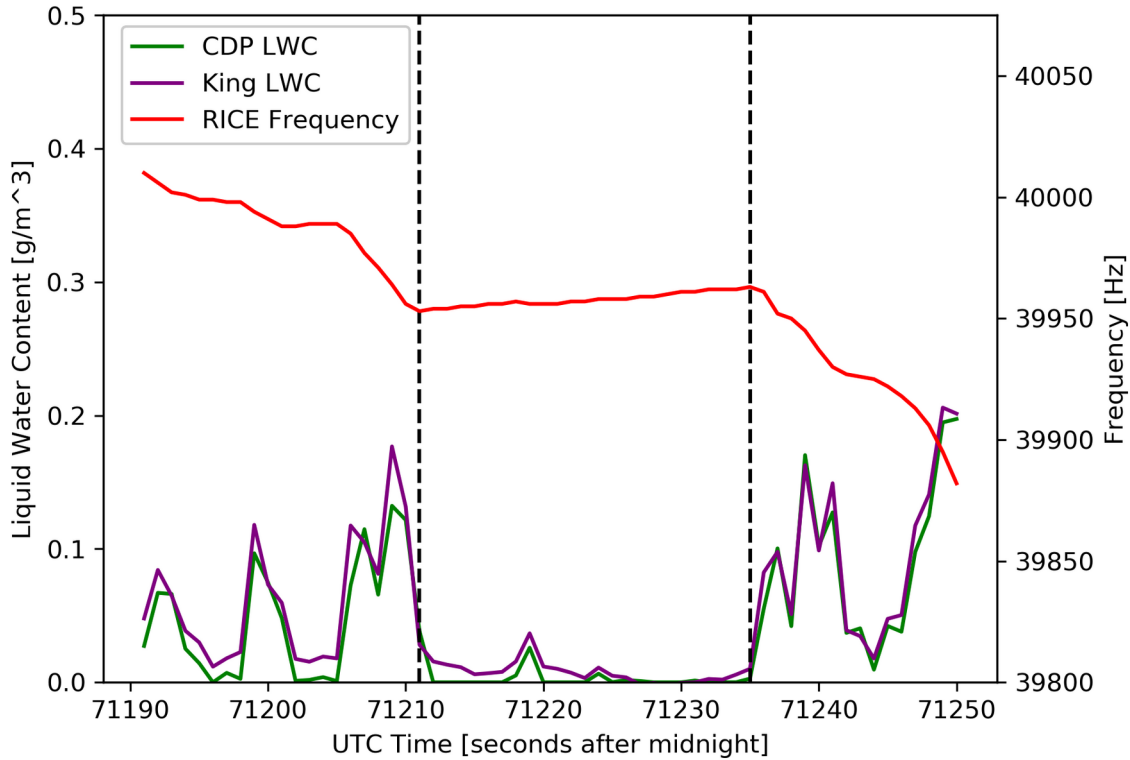


Figure 10: Rosemount Icing Detector frequency and liquid water content from the King Probe and Cloud Droplet Probe at 2/7/2020 from 19:46:31Z to 19:47:36Z.

After the cases were quality-controlled, the dataset was ready for analysis. The RICE SLWC product is calculated by the following equation, modified from Mazin et al (2001):

$$W_m = \frac{-\frac{dF}{dt} \cdot k}{2R_c l U}, \quad (4)$$

where W_m is the SLWC (g m^{-3}), dF/dt is the time derivative of frequency (Hz s^{-1}), k is an empirically-derived constant (g Hz^{-1}), R_c and l are the radius and length of the cylinder (both m), and U is the TAS (m s^{-1}). The change in RICE Probe

Frequency is center differenced in time following the following formula for example time n:

$$\frac{dF}{dt} = \frac{F_{n+1} - F_{n-1}}{2}, \quad (5)$$

where F is the RICE Probe Frequency (Hz). To match the 2-second time period, the LWC products from the King Probe and CDP are separately averaged over the same time period. The two second averaging smooths the data (Fig. 11) and also ensures that the data are not influenced by noise in the signal. The negative dF/dt is divided by the TAS, the diameter of the RICE Probe, and the length of the RICE Probe to match Eq. (4), constituting the RICE Probe response. The RICE Probe response and the smoothed LWC values are combined into scatterplots with the 8 quality controlled cases resulting in 254 seconds of valid data. A linear regression is performed and a trendline forced through the origin is made, and the k constant in Eq. (4) is given by taking the slope of the indicated trendline. The trendline was forced through the origin because a 0 response from the RICE indicates 0 g m⁻³ of SLWC, which would be shown by a value of 0 g m⁻³ for LWC.

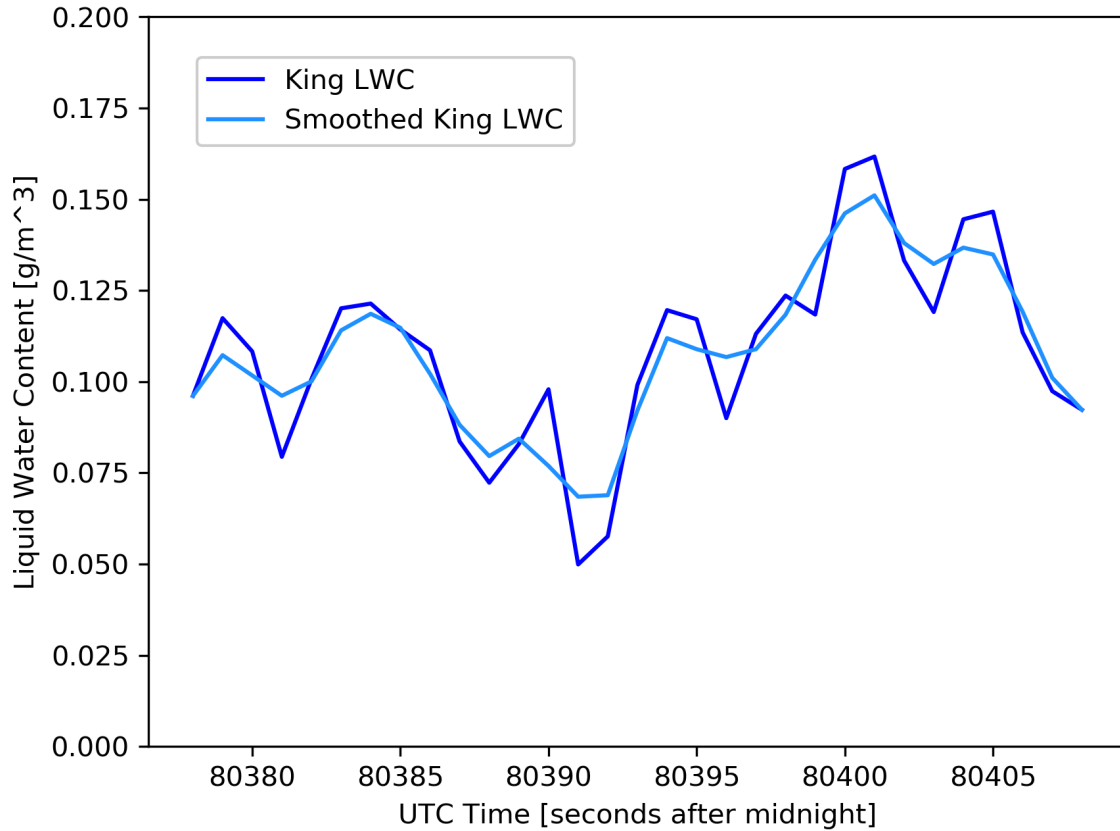


Figure 11: King Probe liquid water content before and after two second averaging at 1/25/2020 from 22:19:38Z to 22:20:20Z.

With the k constant empirically derived in liquid-phase cases, the RICE will likely give accurate measurements in most mixed-phase conditions, because the RICE does not respond to ice particles, unlike the King Probe and CDP (Heymsfield and Miloshevich 1989; Cober et al. 2001a). There is precedent for using a hot wire probe such as the King Probe for icing studies (Bain and Gayet 1982; Mazin et al. 2001) as well as precedent for usage of a forward scattering probe such as the CDP (Heymsfield and Miloshevich 1989). In order to convert the RICE Probe output to accurate SLWC values for an entire flight, a number of filters must be applied. One such filter is a positive frequency change filter. The positive frequency change filter disregards data when the frequency rises with time

due to ice shedding from the probe (naturally or by heating cycle) or sublimating in regions of little to no SLWC. This precludes negative SLWC values. Another filter regarding the heating cycle is the time after the heater has been activated that the probe is too hot to accumulate ice. While the amount of time it takes for the probe to return to thermal equilibrium varies in different environments and between probes, it does not have a known calculation. Thus, there are two options for a filter: manual inspection of data post-flight or setting a static period of time after a cycle to filter out data. While manual inspection of data may preserve more data, it is prohibitively labor intensive. Therefore, the 20 seconds after a sharp rise in frequency (indicating the start of a heater cycle) are disregarded. The length of time is consistent with the approximate values of the length of the cycle as found in Cober et al. 2001b. An example of RICE behavior around a heater cycle is shown in Fig. 5. Finally, a missing data filter is applied to disregard data when the missing value codes are present for any of the following data: the RICE frequency, air temperature, or TAS.

2. Analysis

To ensure that the Rosemount Icing Detector is performing reliably as a SLWC sensor, a series of tests are performed to determine the ideal conditions for optimal probe performance. The following conditions are analyzed while holding other conditions constant to attempt to isolate the independent variable: temperature, pitch angle, roll angle, true air speed, mean volume diameter, and total particle concentration. The SLWC product is compared to the CDP LWC product and the King LWC product. It is acknowledged that the CDP and King respond to ice particles while the RICE does not, and that not all LWC is supercooled, making SLWC an inherently limited product compared to LWC. However, without any

other SLWC products to compare to, the LWC products from the CDP and King are the best comparison products available.

Given that the SLWC product desired depends on the water being at a supercooled temperature, a temperature analysis is the highest priority. While the Cober et al. (2001b) study provides some guidance for a temperature threshold, there is value in independently testing temperature thresholds with the IMPACTS 2020 dataset to quantify the effect of temperature on a newer RICE Probe operating at a higher airspeed. While a direct calculation of the Ludlam limit would be ideal, there is considerable difficulty in measuring or parameterizing all of the variables and constants within the Ludlam limit equation. Therefore, a number of temperature filters are tested and the correlation between known LWC values and RICE SLWC values are calculated. The ideal temperature filter maximizes accuracy while minimizing data lost.

When studying the RICE Probe data in past studies such as Heymsfield and Miloshevich (1989), it is common practice to only consider straight and level flight. Straight and level flight is measured in two ways, pitch angle and roll angle. Pitch angle is the aircraft's rotation about the y-axis (or transverse axis), while the roll angle is the aircraft's rotation about the x-axis (or longitudinal axis). The pitch angle is chiefly associated with ascent and descent, as rotating positively about the y-axis (and thus, having a positive pitch angle) places the nose of the aircraft higher than the wings and causes ascent, and vice versa for negative rotation about the y-axis and negative pitch angle. Roll angle is chiefly associated with banking left and right, as a positive rotation about the x-axis (and positive pitch angle) places the port (left) wing above the starboard (right) wing, causing a bank to the right, and vice versa for negative rotation about the x-axis and negative roll angle. Largely positive and negative pitch and roll angles tend to be avoided in airborne data analysis due to concerns over changes in the airflow, such as some part of the

aircraft structure “shadowing” a probe and sweeping out the particles in front of a probe such that the probe is sampling a sample volume that is not representative of the surrounding atmosphere. The effects of pitch and roll angle will likely be dependent on the aircraft used and the mounting position of the instruments used in comparison. This analysis applies to the NASA P-3 Orion with the RICE Probe mounted on the starboard side of the fuselage and the CDP and King Probe mounted under the port wing.

Another analysis is done to test the effect of airspeed on the temperature threshold. The Ludlam limit is dependent on not only temperature but also airspeed. Faster airspeeds increase the volume of water encountered by the RICE Probe at a given time, potentially pushing the RICE Probe over the Ludlam limit. In theory, at slower air speeds, the RICE Probe can more accurately sample higher SLWC environments. The effect of TAS on RICE Probe measurements is demonstrated by comparing the RICE and LWC at temperature values near the temperature filter derived in the previous tests.

Another test of RICE performance will be to determine if there is a low bias in large particle size regimes, similar to the King’s low bias in large droplet size environments. The RICE Probe SLWC is compared to the CDP LWC in a variety of mean volume diameters as calculated by the CDP and 2D-S to determine the performance in different particle size regimes. The MVD is the mean particle diameter weighted by the particle volume and is calculated by:

$$MVD = \frac{\sum_{i=1}^m V_i d_i}{\sum_{i=1}^m V_i}, \quad (6)$$

where V_i is the volume of a particle of the bin midpoint of size bin i (m^3) and d_i is the diameter of a particle of the bin midpoint of size bin i (m). Similarly to

particle size, the RICE Probe is tested to see if there is a reduction in signal in large particle concentrations. When analyzing bulk microphysical parameters, it is helpful to construct a spectrum that is representative the entire environment of particles. As the CDP can only detect particles below 50 μm , it is necessary to merge the spectrum of the CDP with that of the 2D-S Probe and the HVPS-3. The merged spectrum consists of the first 28 bins of the CDP (bin midpoints ranging from 2.5 μm to 45 μm), bins 5-24 of the 2D-S (bin midpoints ranging from 50 μm to 950 μm) and bins 5-28 of the HVPS-3 (bin midpoints ranging from 1,100 μm to 27,500 μm). In typical mixed phase environments, the normalized spectrum (particle concentration divided by the bin width) is bimodal (Fig. 12). The smaller particle size peak is assumed to be liquid droplets while the larger particle size peak is assumed to be ice crystals. The assumption is supported by evidence in the 2D-S and HVPS-3 imagery (Fig. 13, Fig. 14) with the presence of small quasi-circular particles on the 2D-S coexisting with much larger ice crystals on both the 2D-S and HVPS-3. For example, a capped column that takes up most of the width of the 2D-S image takes up a fraction of the width of the corresponding HVPS-3 image. Similarly, the small round particles on the 2D-S that are assumed to be supercooled liquid water drops are completely absent on the HVPS-3. Since only water particles are desired, if water droplets are not shown on the HVPS-3, that data can be safely omitted. Given how the gap between the two peaks in the spectrum is most commonly at around 200 μm , size bins above bin 14 on the 2D-S (midpoint of 200 μm) are omitted. While it is acknowledged that some ice crystals smaller than 200 μm might contaminate the dataset, omitting the larger peak in the particle size spectrum minimizes the majority of ice contamination. With the spectrum narrowed down to just sub-200 μm particles, the total concentration and MVD are recalculated.

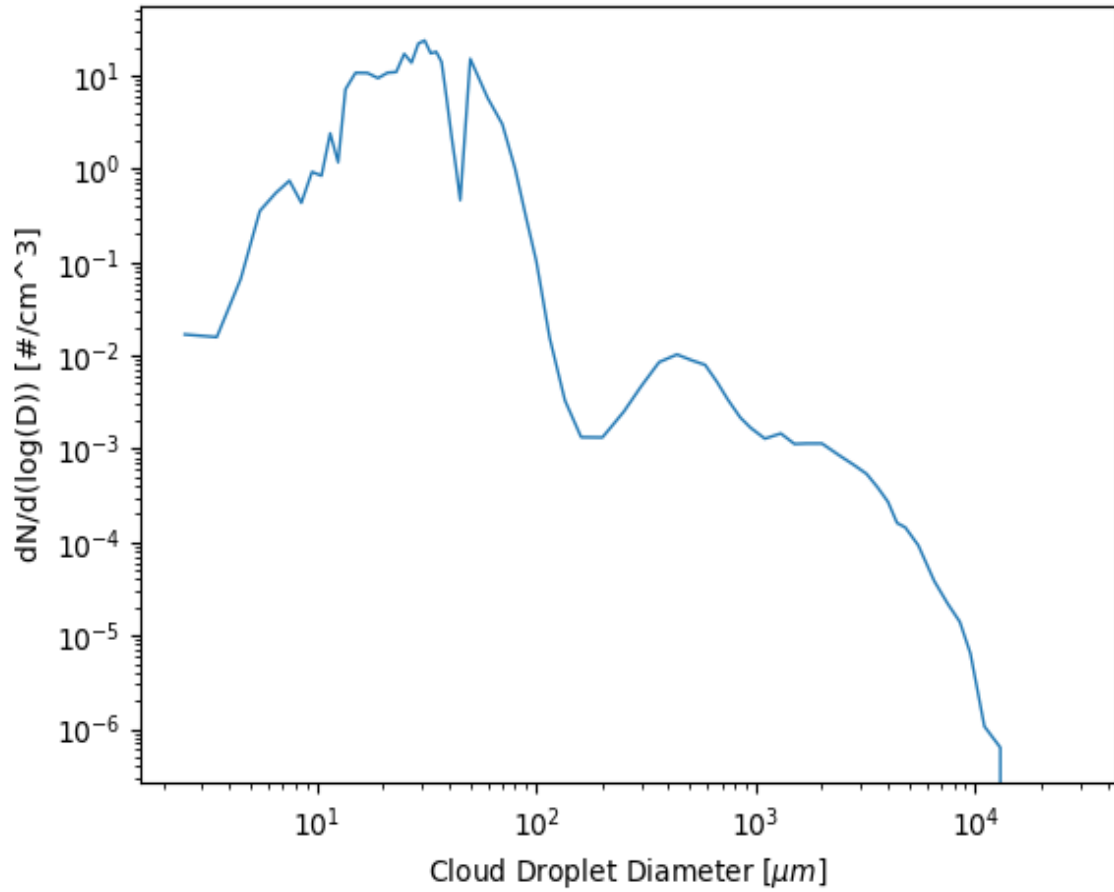


Figure 12: Merged particle size distribution spectrum from the Cloud Droplet Probe, Two Dimensional Stereo Probe, and High Volume Precipitation Spectrometer Version 3 for a in-cloud period at 2/5/2020 from 23:43:16Z to 23:46:10Z.

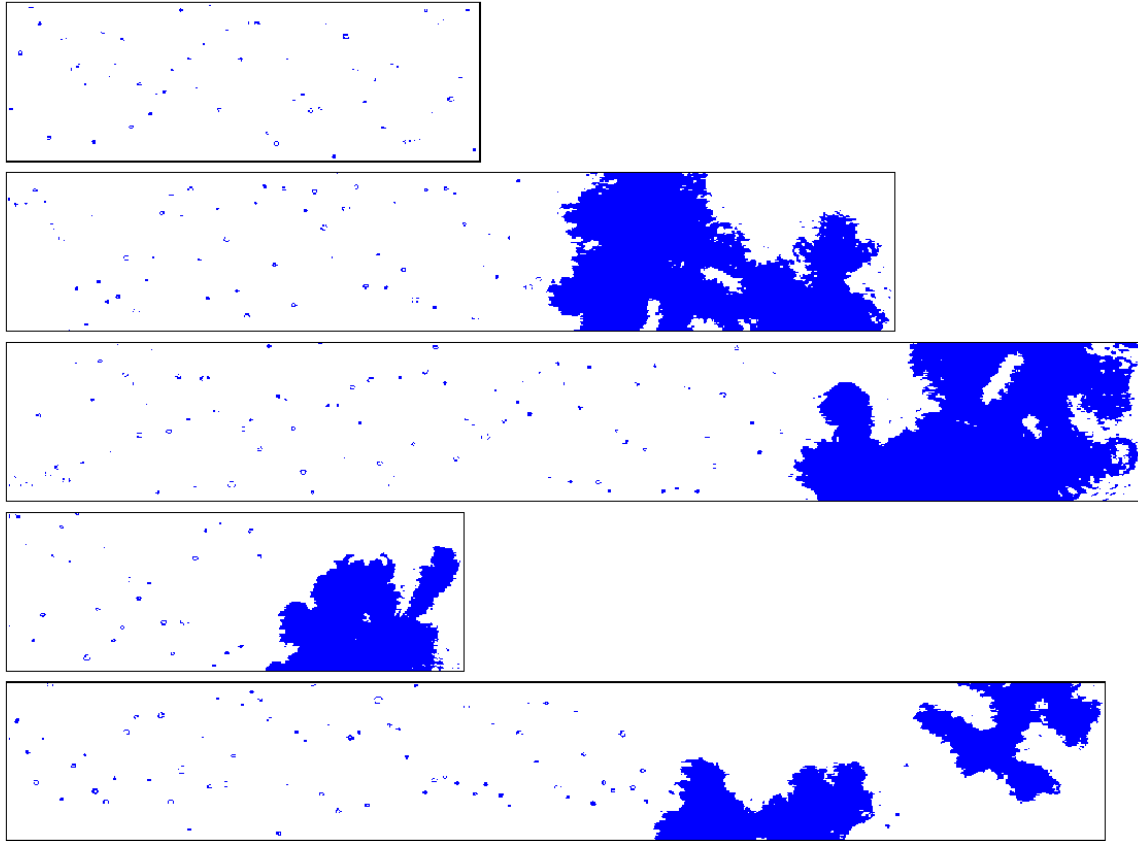


Figure 13: Two Dimensional Stereo Probe imagery at 2/5/2020 23:46Z. Pixel resolution is $10\ \mu\text{m}$, each strip is 128 pixels tall for a scale of $1,280\ \mu\text{m}$ in the y axis for each strip. Periods of time with no diodes shadowed are omitted.

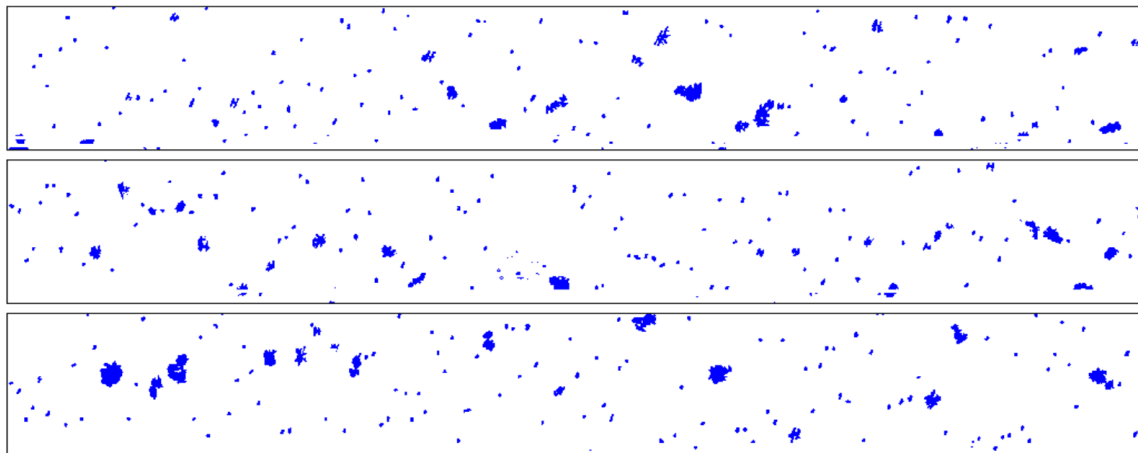


Figure 14: High Volume Precipitation Spectrometer imagery at 2/5/2020 23:46Z. Pixel resolution is $150\ \mu\text{m}$, each strip is 128 pixels tall for a scale of $19,200\ \mu\text{m}$ in the y axis for each strip. Periods of time with no diodes shadowed are omitted.

Finally, the minimum detection threshold is analyzed. Regarding the analog voltage models of the RICE Probe, there is some debate in the literature regarding the minimum detection threshold for the probe. Heymsfield and Miloshevich (1989) settled on a value of 0.002 g m^{-3} . Strapp et al. (1999) found that at 200 m s^{-1} , the minimum SLWC detection threshold could be as high as 0.06 g m^{-3} . Jackson et al. (2001b) claim that the minimum detection thresholds in Heymsfield and Miloshevich (1989) and Strapp et al. (1999) are “confused” and that “there is no minimum level of LWC needed before the [RICE Probe] can detect.” Mazin et al. (2001) found the values were dependent on humidity, temperature, and airspeed but characteristic values were 0.005 g m^{-3} for an airspeed of 100 m/s and 0.01 g m^{-3} at an airspeed of 200 m s^{-1} (with $T > -20 \text{ }^\circ\text{C}$). Cober et al. (2001b) found the value to be as high as 0.017 g m^{-3} on the Environment Canada Convair-580. The resolution of the digital frequency model used in the IMPACTS 2020 field campaign is an inherently limiting factor that leads to a nonzero minimum detection threshold.

CHAPTER 4

RESULTS

1. SLWC Derivation

As shown in the scatterplots in Fig. 15 and Fig. 16, the k value when comparing the RICE and King Probes is $4.292 \times 10^{-4} \text{ g Hz}^{-1}$ while the k value when comparing the RICE Probe and the CDP is $4.752 \times 10^{-4} \text{ g Hz}^{-1}$. Given the difference between the two values, a choice is made regarding which k value to use. While both the King Probe and the CDP have their drawbacks and advantages, the CDP is chosen as the preferred instrument for comparison. The King Probe may be biased because the baseline voltage can drift when in cloud and in changing density, TAS, or altitude. The CDP does not suffer from such a drifting baseline. The scale of the storms analyzed in the 2020 NASA IMPACTS IOPs made for extended periods of time in-cloud, leaving a high potential for the King Probe to suffer from a baseline voltage drift bias larger than the biases that the CDP suffers from. With a k value derived, Eq. (4) can be used in many mixed phase conditions outside of the cases described above.

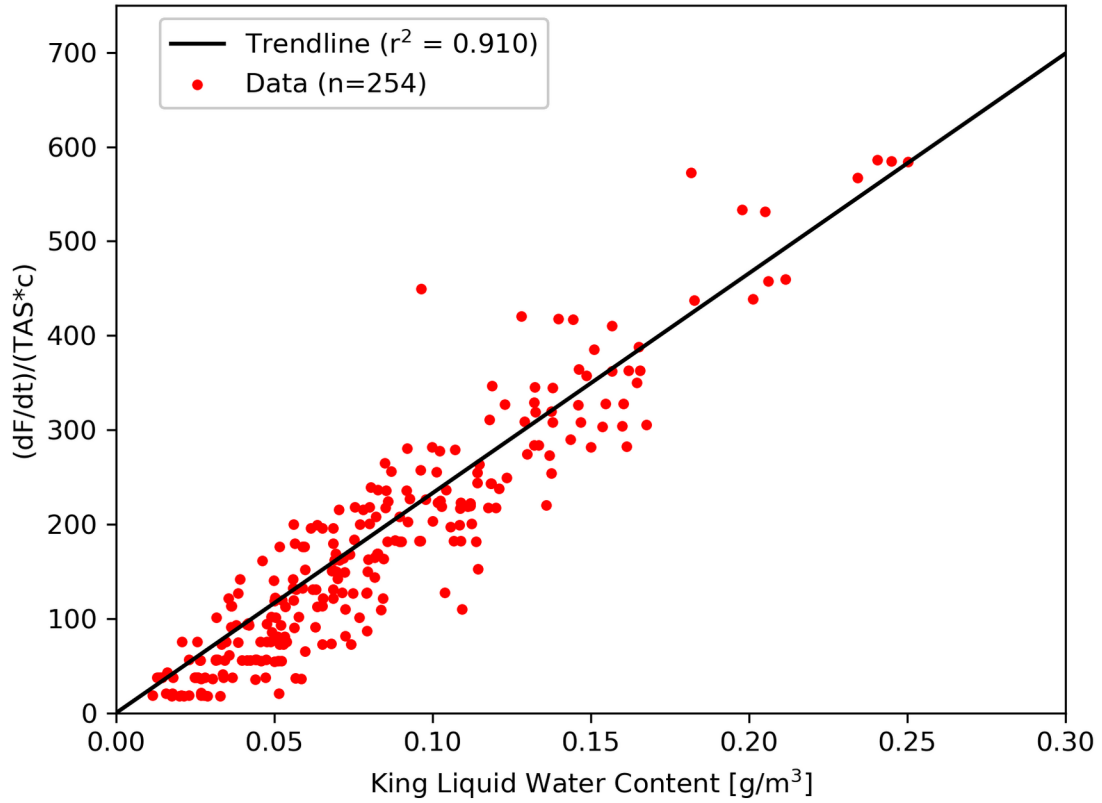


Figure 15: Scatterplot of all 8 cases comparing the King Probe liquid water content to the Rosemount Icing Detector change in frequency divided by the true air speed and the probe diameter and length (c). The trendline here has a slope of 4.292×10^{-4} , which is the empirical k constant in Hz^{-1} .

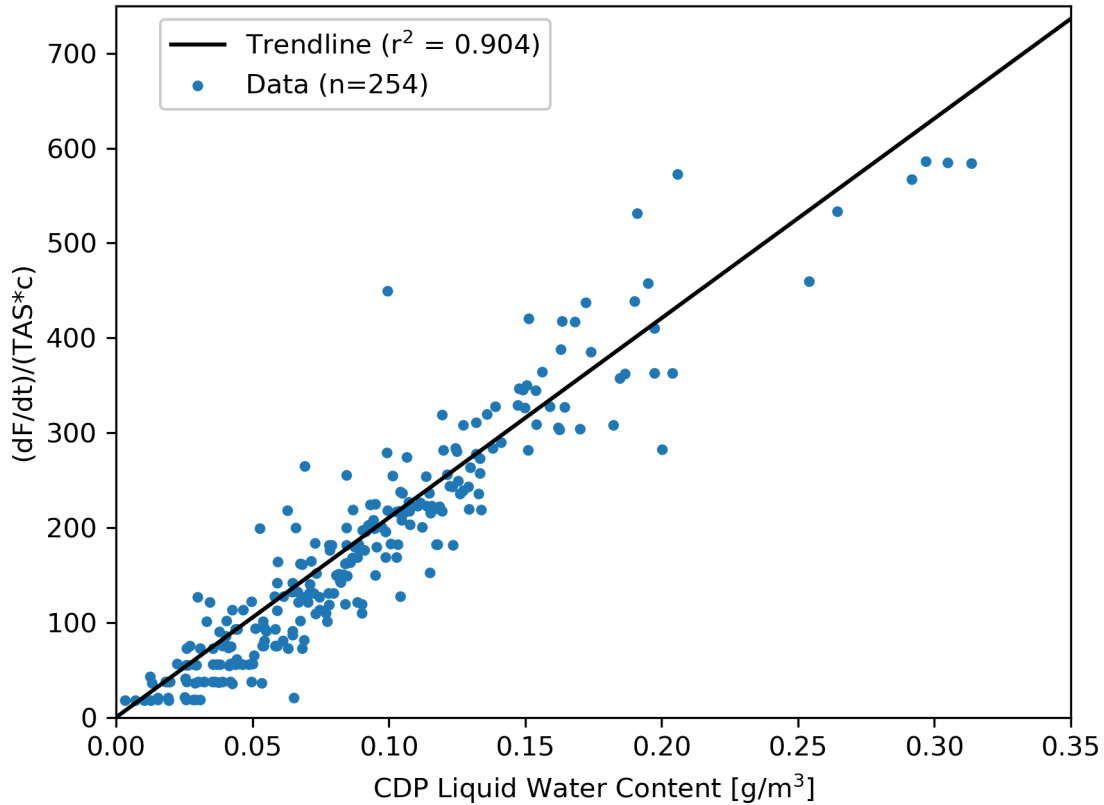


Figure 16: Same as Fig. 15 but with the Cloud Droplet Probe instead of the King Probe. The trendline here has a slope (and thus, the empirical k constant is) equal to $4.752 \times 10^{-4} \text{ g Hz}^{-1}$.

2. Environmental Tests Overview

With all of the unknowns in the equation for SLWC resolved, the SLWC product can be applied to conditions throughout the IMPACTS 2020 campaign, including mixed-phase conditions, provided that supercooled water is present. To evaluate the performance of the RICE Probe as a SLWC-measuring probe, a number of tests are performed and scatterplots made to compare to the simultaneous LWC measurement from the CDP while the RICE Probe and CDP are both showing a nonzero signal. Within each test, a set of filters will be tested for a given independent variable and a linear regression performed to measure if

the given filters improve agreement between the RICE Probe and the CDP water content measurements. It is acknowledged that the CDP LWC will be biased somewhat by the ice crystals present in mixed-phase conditions, but there are no probes present to compare the RICE Probe to that are not biased by ice, so the CDP is the best comparison available. In all scatterplots, the 1:1 line is plotted in black.

3. Temperature

As discussed earlier, there are considerable challenges in exact calculations of the Ludlam Limit, but the strongest influence on the Ludlam Limit is the air temperature. Therefore, several air temperatures are tested to determine the point at which the RICE Probe agreement with measured LWC begins to plateau with decreasing temperature. An ideal temperature filter maximizes data preserved while maintaining high agreement.

Figure 17 shows a four-panel plot of scatterplots of the RICE Probe SLWC and CDP LWC with temperature filters at 12 °C, 0 °C, -3 °C, and -10 °C. Figure 18 shows a plot of the r^2 and percentage of observations present across different temperature filters when comparing the Rice Probe and CDP. The percentage of observations decreases in a mostly linear fashion with decreasing temperature such that 72% of all observations remain at a temperature filter of -2 °C and below and 51% of observations remain at a temperature filter of -6 °C and below. With temperature filters of -3 °C, r^2 values only increase marginally while observations continued to decrease in a linear fashion. While the r^2 value increases from 0.819 to 0.853 going from -3 °C to -10 °C, the amount of valid observations drops from 12,244 to just 6,805 across the four flights with valid CDP and RICE Probe data. With the cost of potentially thousands of data points for such marginal agreement

increases, $-3\text{ }^{\circ}\text{C}$ was found to be an acceptable upper temperature threshold and was applied to all following tests.

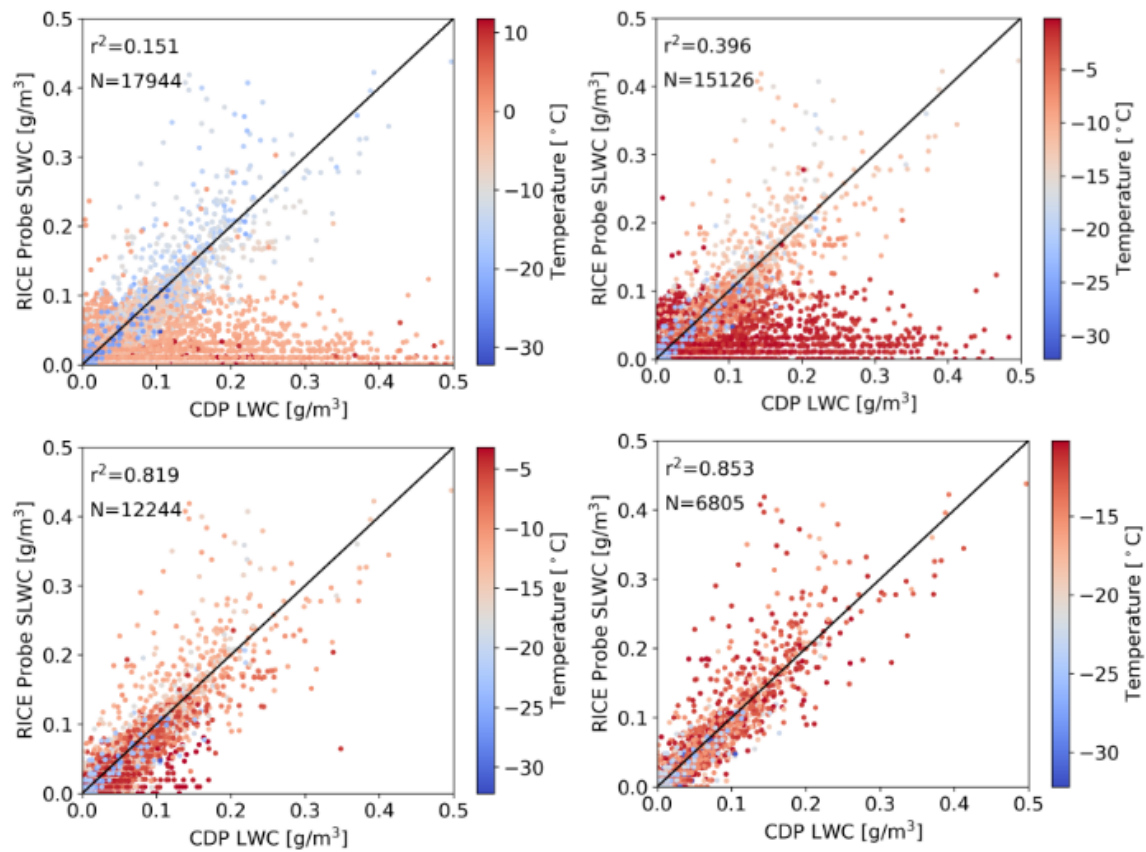


Figure 17: Scatterplots of the Rosemount Icing Detector supercooled liquid water content and Cloud Droplet Probe liquid water content over the four flights in IMPACTS 2020 in which both probes had valid data. From top left clockwise: $12\text{ }^{\circ}\text{C}$ and below, $0\text{ }^{\circ}\text{C}$ and below, $-10\text{ }^{\circ}\text{C}$ and below, and $-3\text{ }^{\circ}\text{C}$ and below.

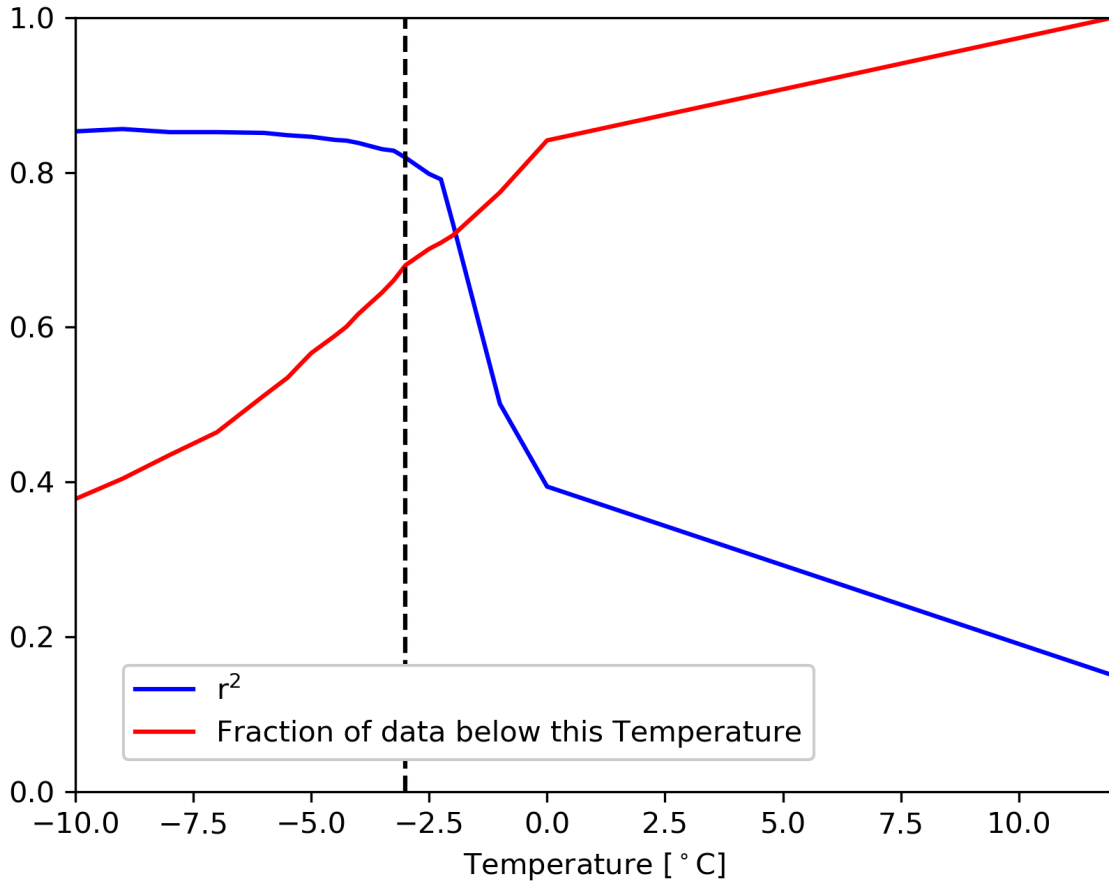


Figure 18: Plot of the correlation coefficient of various temperature thresholds and the fraction of the total dataset that each threshold represents. The maximum temperature in this dataset is 12 °C.

4. Pitch Angle and Roll Angle

Figure 19 shows a four-panel plot of scatterplots of the RICE Probe SLWC and CDP LWC with all pitch angles, pitch angles greater than 2°, pitch angles less than -2°, and pitch angles between -2° and 2°. While the highest percentage of pitch angles are slightly negative (Fig. 20), for a typical flight the 5th and 95th percentile of data are between -2° and -3° and between 2° and 3° respectively. The negatively pitched data points (-2° and below) are remarkably well correlated, with a 0.934 r^2 value. Positive pitch (2° and above), however, is lower at a r^2 value

of 0.654. Figure 21 shows a scatterplot similar to those in Fig. 19 but filtered for pitch angles of 3° and above. The r^2 value is even lower at 0.64, and at 477 data points, and with little discernible pattern to the spread in that graph, 3° is decided as the upper limit for pitch angle, with no lower limit being deemed necessary for a fuselage-mounted RICE Probe on the NASA P-3 Orion. It is worth noting that the error with high pitch angles is not as significant as the error caused by warm temperatures, but the error reduction by setting that limit is not negligible.

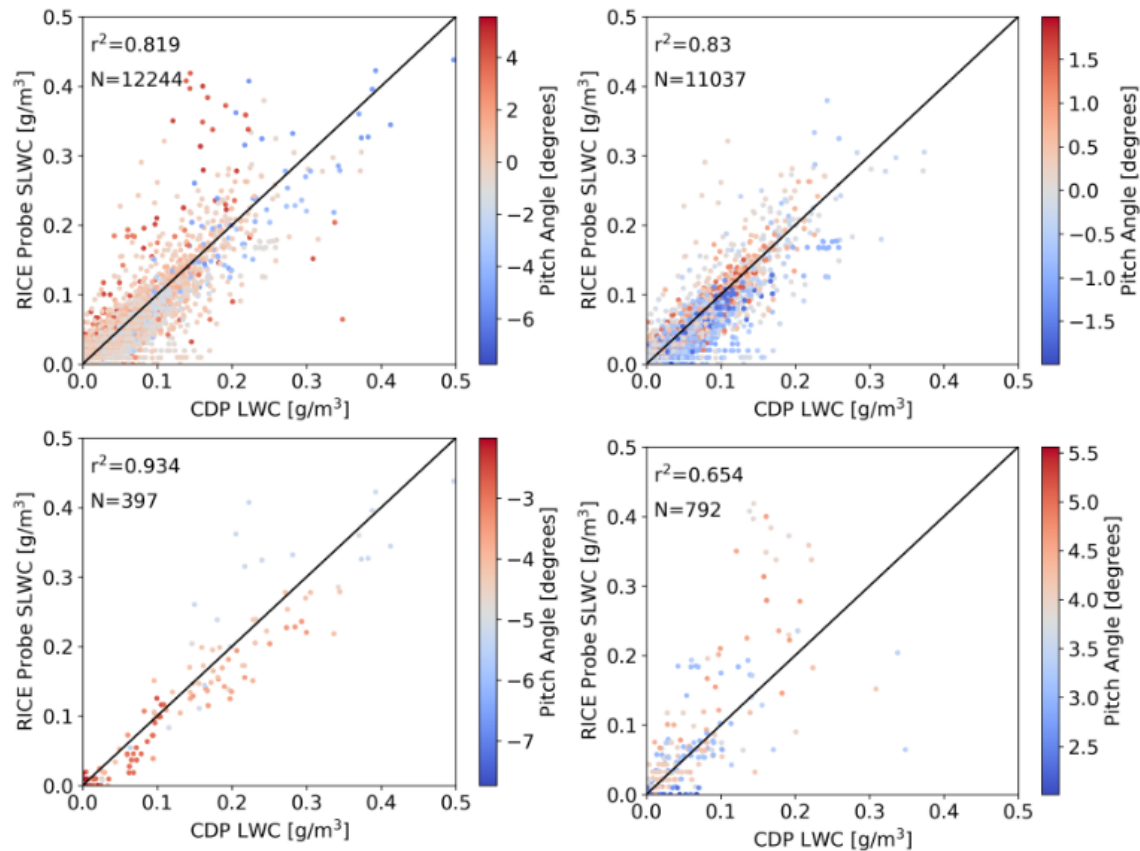


Figure 19: Scatterplots of the Rosemount Icing Detector supercooled liquid water and Cloud Droplet Probe liquid water content over the four flights in IMPACTS 2020 in which both probes had valid data. From top left clockwise: all pitch angles, -2° to 2°, 2° and above, and -2° and below.

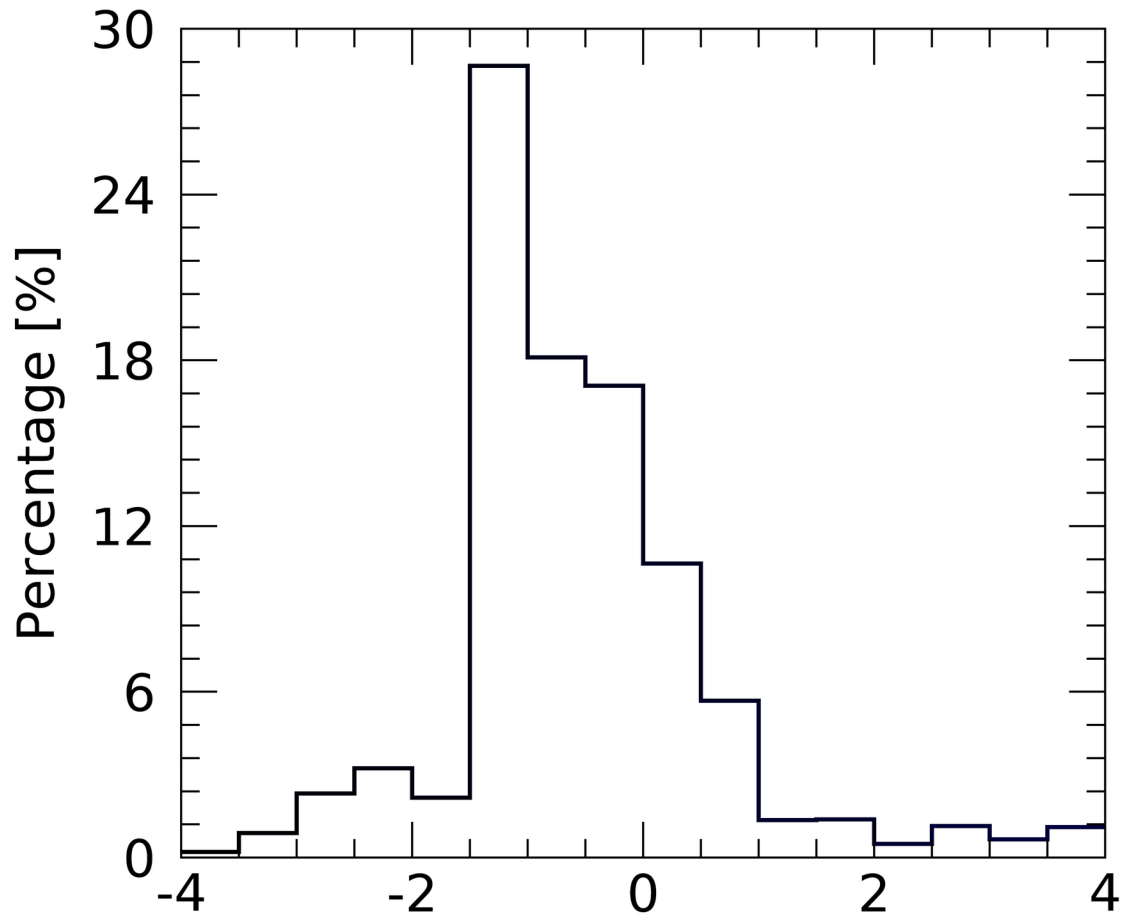


Figure 20: Histogram of the pitch angles over the course of the 1/25/2020 flight. The x axis is the pitch angle, with units of degrees.

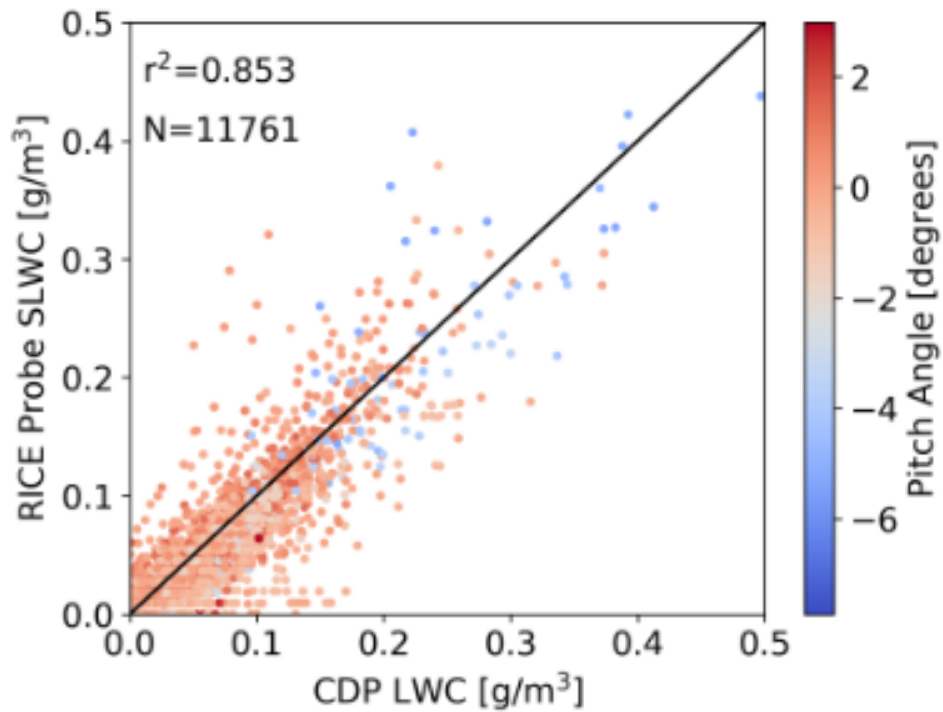
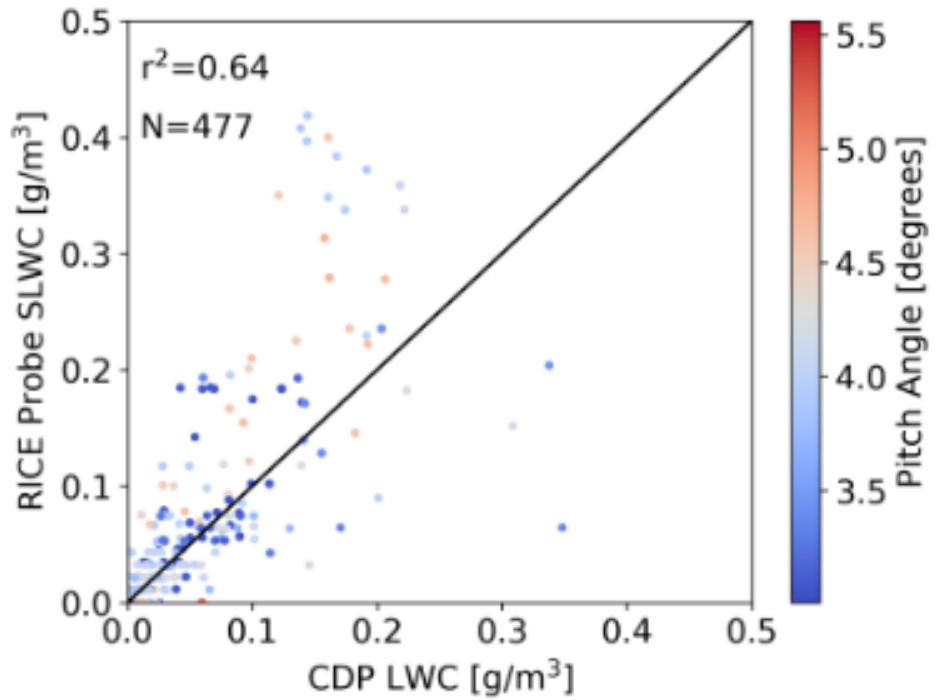


Figure 21: Scatterplot of Rosemount Icing Detector supercooled liquid water content and Cloud Droplet Probe liquid water content over the four flights with valid data from both probes, limited to pitch angles of 3° and above (top), and 3° and below (bottom).

Figure 22 shows a four-panel plot of scatterplots of the RICE Probe SLWC and CDP LWC with all roll angles, roll angles greater than 2° , roll angles less than -2° , and roll angles between -2° and 2° . For a typical flight, the majority of roll angles are centered around 0° (Fig. 23), and as the tails of the histogram are approximately the same as for pitch angles, $\pm 2^\circ$ was still a logical choice to search for outliers. For a fuselage-mounted RICE Probe, neither positively or negatively tilted roll angles indicate a large spread in the data, therefore no angle limit is implemented.

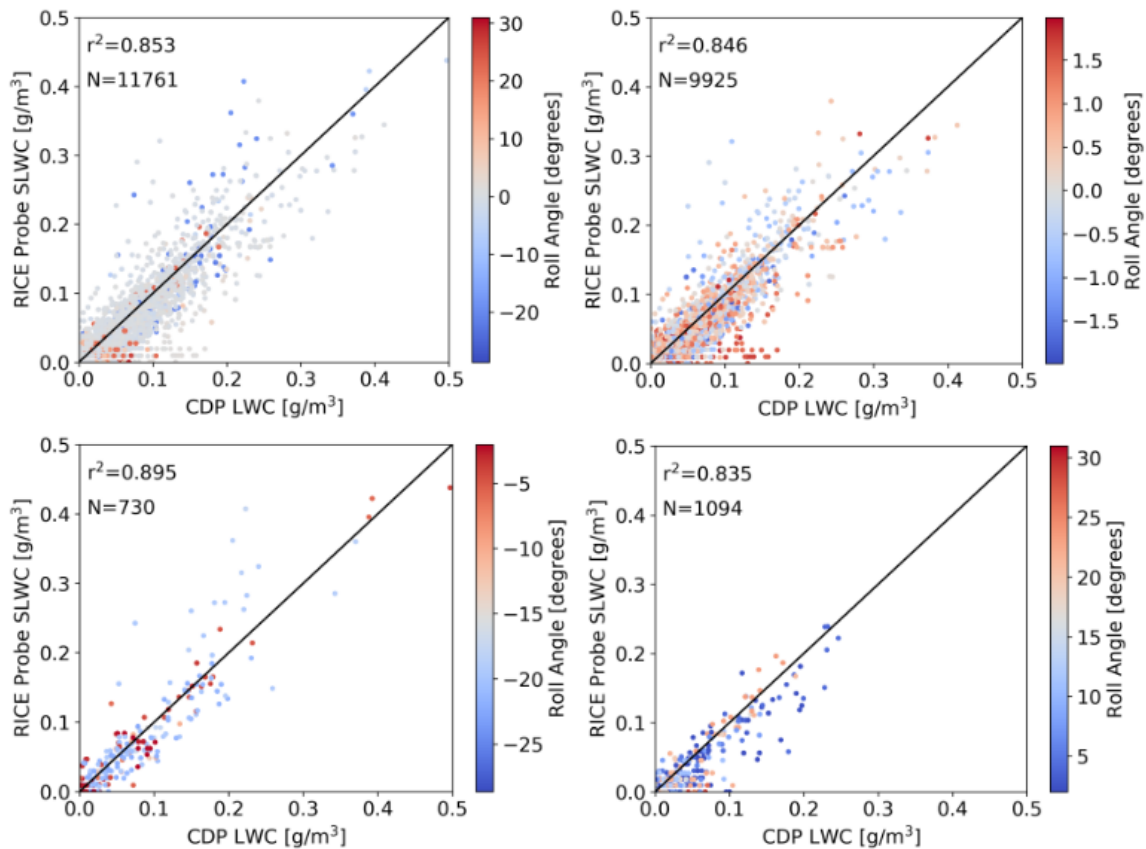


Figure 22: Scatterplots of the Rosemount Icing Detector supercooled liquid water content and Cloud Droplet Probe liquid water content over the four flights in IMPACTS 2020 in which both probes had valid data. From top left clockwise: all roll angles, -2° to 2° and above, and -2° and below.

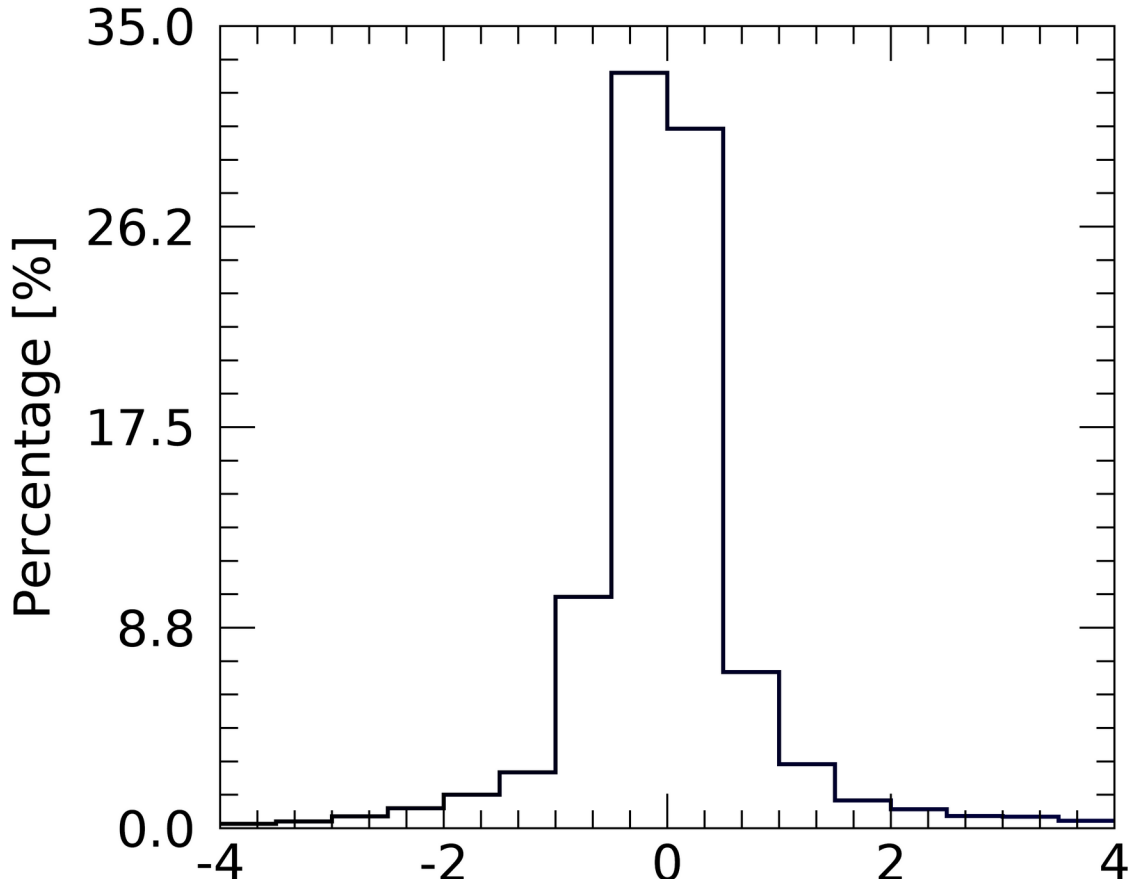


Figure 23: Histogram of roll angles throughout the course of the 2/7/2020 flight. The x axis is roll angle, with units of degrees.

5. True Air Speed

Figure 24 shows a scatter plot of the RICE Probe SLWC and CDP LWC products in the temperature range of -5 °C to -3 °C, the warmest 2 degrees still within the established acceptable temperature filter. The r^2 value is quite low, but when a maximum TAS filter of 150 m s^{-1} is applied (Fig. 25), the r^2 value recovers notably. However, it is worth noting that the sample size is small in relation to the previous scatterplots and the (S)LWC values are quite low. 150 m s^{-1} represents the bottom quartile of TAS's in a typical flight (Fig. 26). Since the data lines up well with established theory, it is likely that the trend is genuine, but confidence

would be higher with more data. Figure 27 shows that the trend of lower TAS increasing RICE Probe performance disappears as the environment approaches freezing, as in the -3 °C to -2 °C range shows no discernible relation between TAS and the drop-off in RICE Probe signal. However, because agreement is still good regardless of airspeed in cold temperatures (Fig. 28), no airspeed limits are necessary.

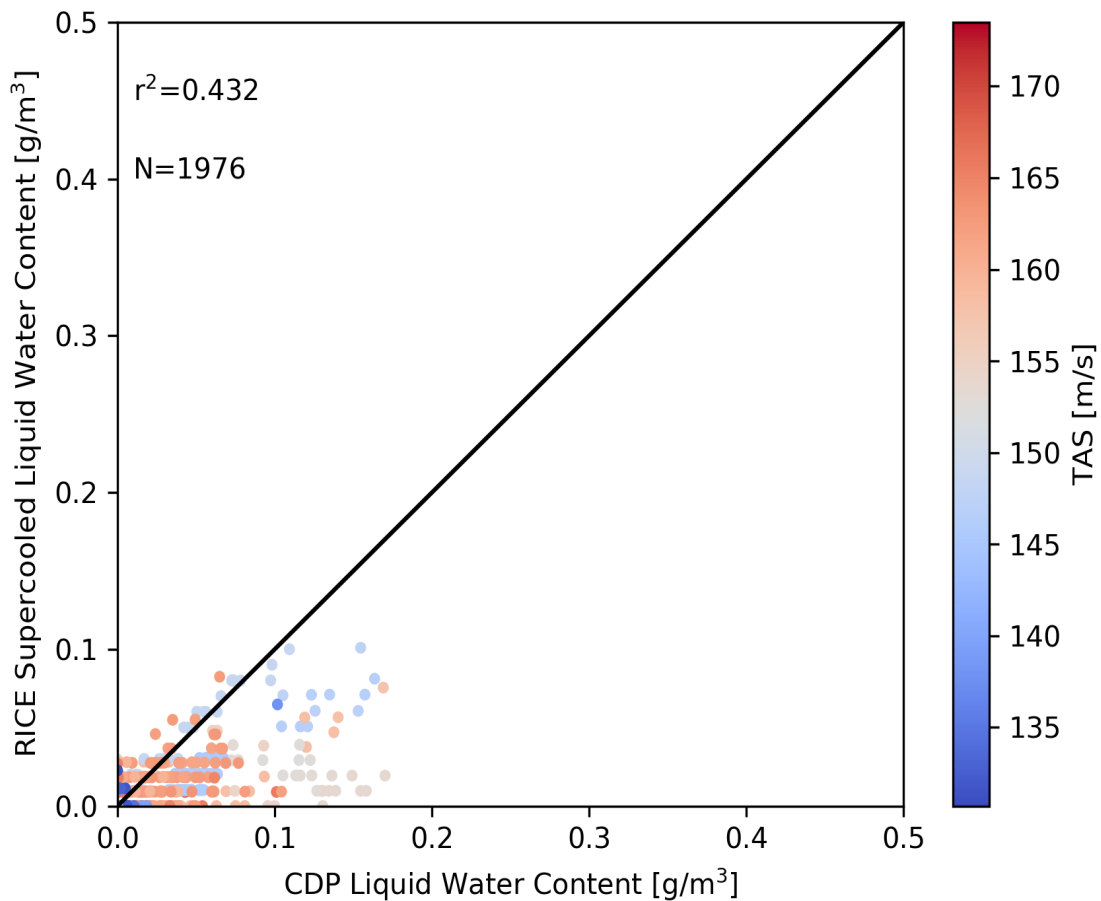


Figure 24: Scatterplot of Rosemount Icing Detector supercooled liquid water content and Cloud Droplet Probe liquid water content scatterplot in the range of -5 °C to -3 °C.

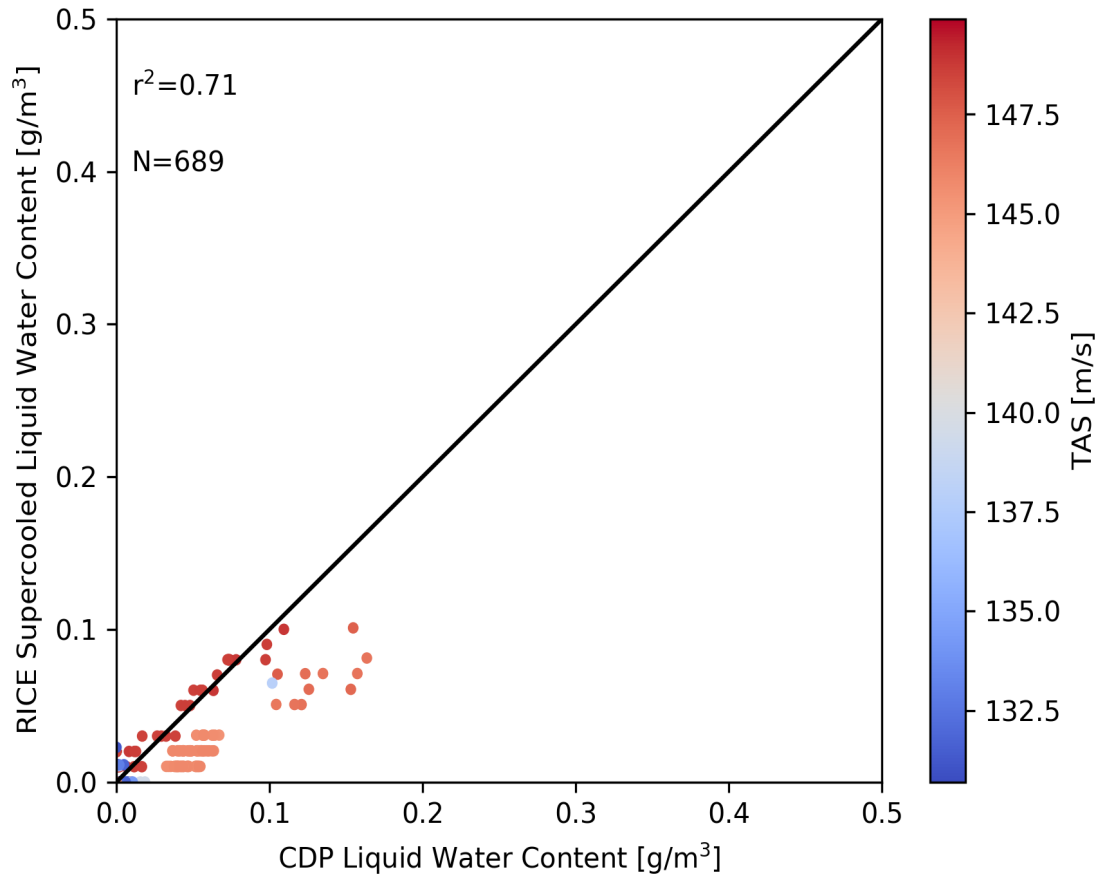


Figure 25: Same as Fig. 24, but with a maximum true air speed threshold of 150 m s^{-1} applied.

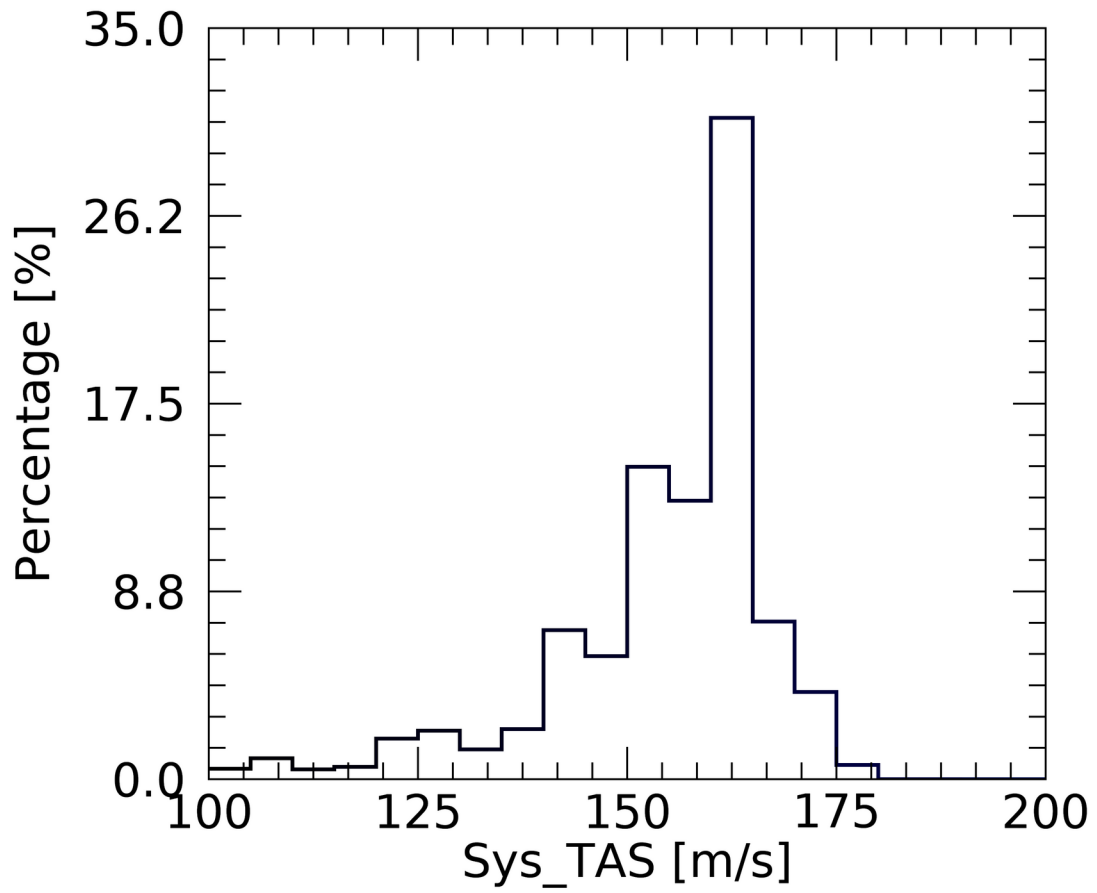


Figure 26: Histogram of true airspeed throughout the 1/25/2020 flight.

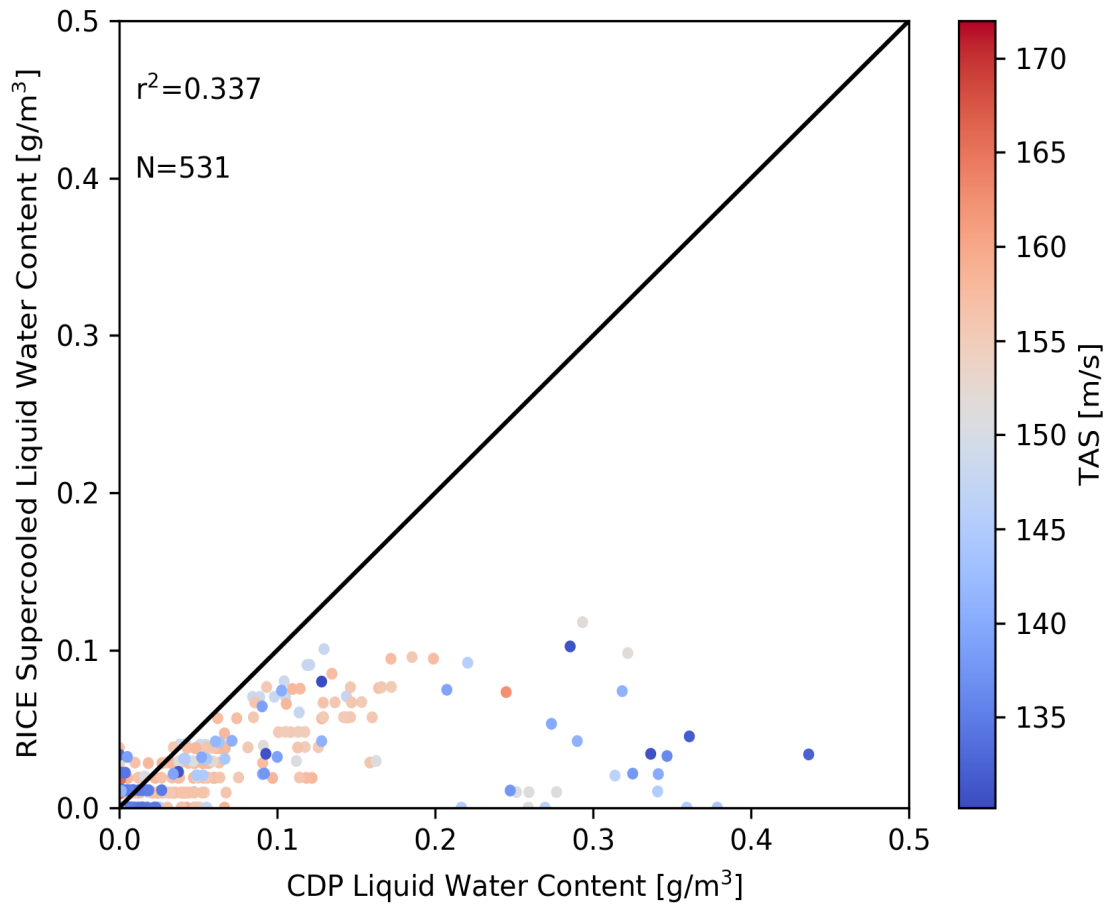


Figure 27: Same as Fig. 24, but in the temperature range of $-3\text{ }^\circ\text{C}$ to $-2\text{ }^\circ\text{C}$.

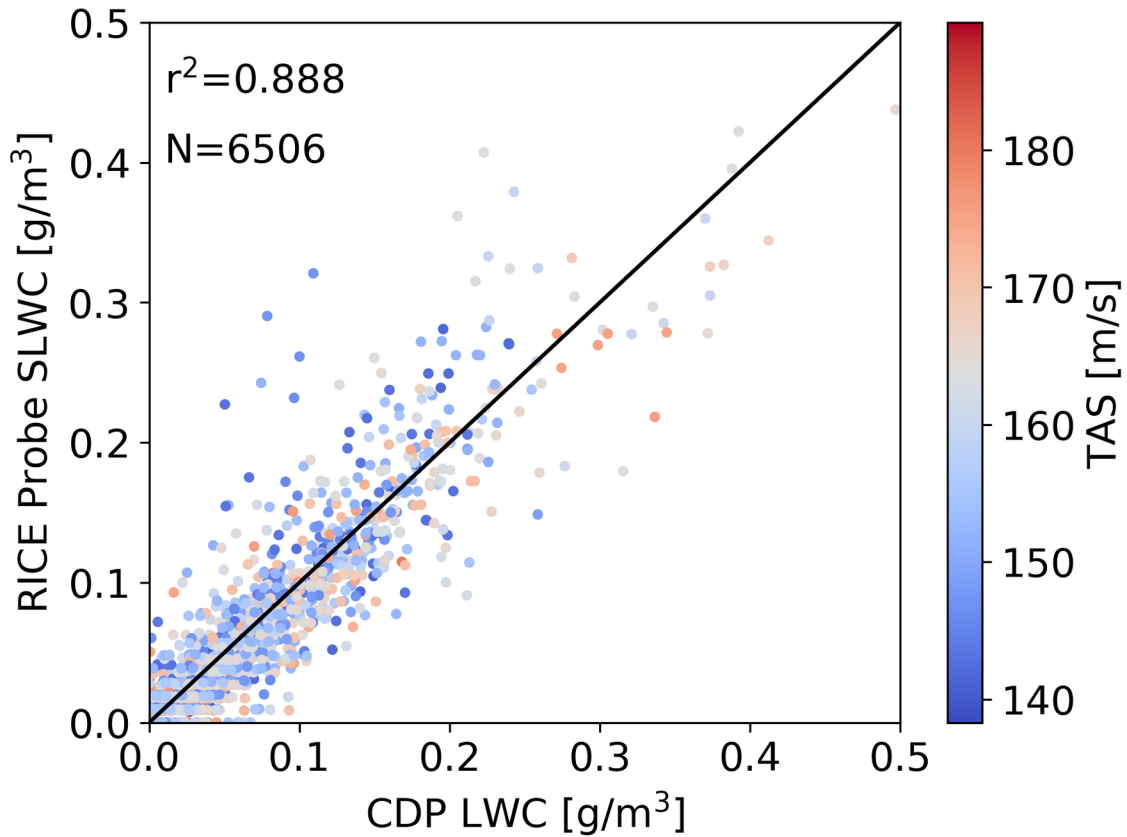


Figure 28: Same as Fig. 24 but with temperatures below -10 °C.

6. Total Particle Concentration and Mean Volume Diameter

The final two variables to test for effects on the RICE Probe SLWC and CDP LWC are total particle concentration and mean volume diameter (MVD) for particles below 200 μm as measured by the CDP and 2D-S Probe. Figure 29 shows the scatterplots of RICE Probe SLWC and CDP at various concentration limits. Little to no pattern is present when analyzing the lower concentrations, indicating that either the RICE Probe and CDP are both performing well, or are both subject to similar biases. At concentrations above 10^8 m^{-3} , the RICE Probe and CDP both read water contents below 0.1 g m^{-3} . While initially it might be expected that higher concentration would lead to higher water content, this is not

observed. The low water contents corresponding with high concentrations are because the counts are chiefly in the lower size bins. During a period of icing conditions from 22:45Z to 22:58Z on the 2/5/2020 flight (Fig. 30), the highest concentration values corresponded with MVD values below 25 μm (Fig. 31), leading to lower water content values than expected. There is some indication that at concentrations larger than 10^8 m^{-3} , the RICE Probe might be underrepresenting the environment relative to the CDP, as all of the points on the scatterplot fall below the 1:1 line. The evidence is contrary to the expectation that the CDP is expected to undercount at large concentrations due to any coincidence bias that is not accounted for in the data processing software, and thus the RICE would be sampling LWC higher. However, at only 36 seconds of data between the four available flights with concentrations larger than 10^8 m^{-3} , the sample size is too small to draw a conclusion.

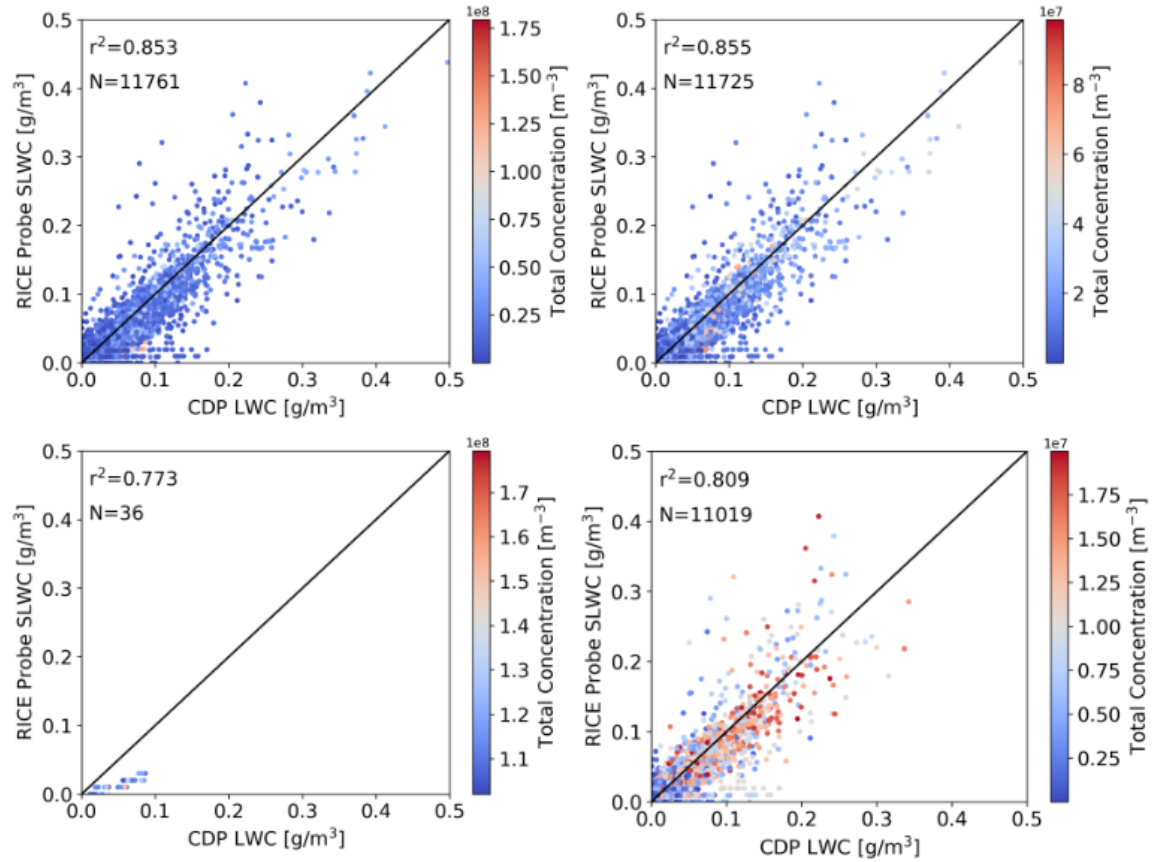


Figure 29: Scatterplots of the Rosemount Icing Detector supercooled liquid water content and Cloud Droplet Probe liquid water content. Concentration limits, from top left, clockwise: no limit, 10^8 m^{-3} and less, $2 \times 10^7 \text{ m}^{-3}$ and fewer, 10^8 m^{-3} and greater.

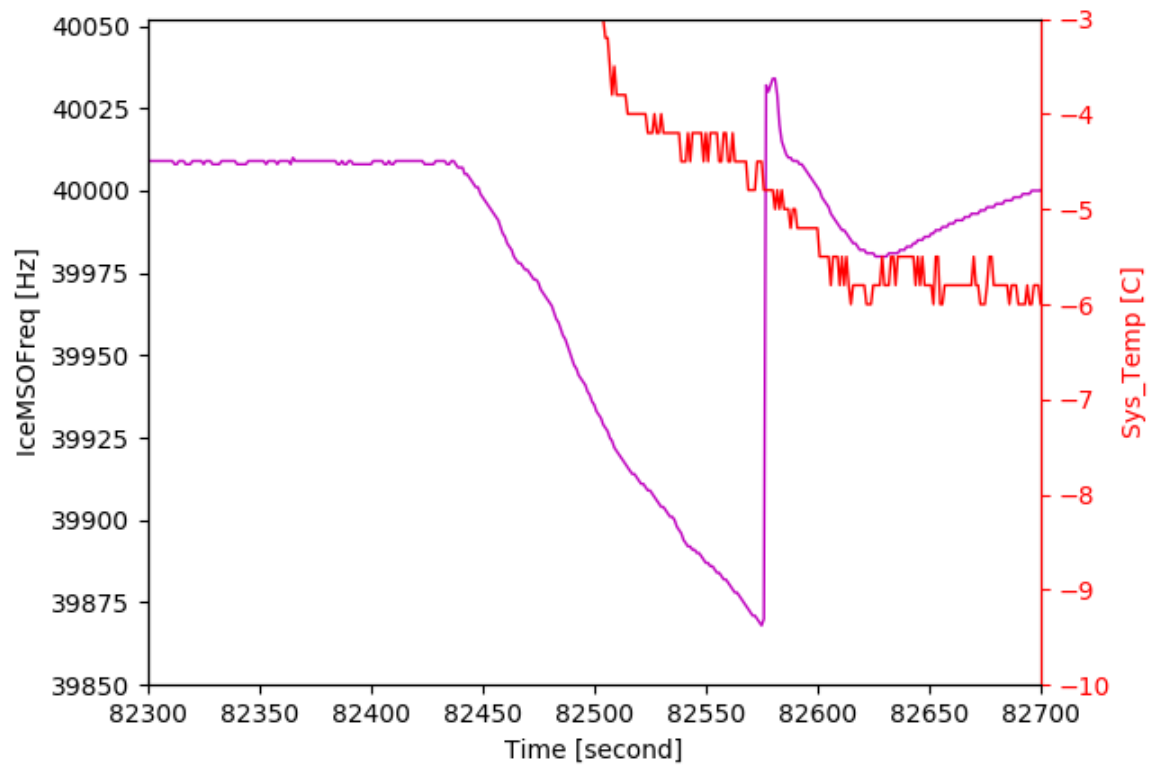


Figure 30: RICE Probe frequency (magenta) and air temperature (red) from 22:52Z to 22:58Z during the 2/5/2020 flight.

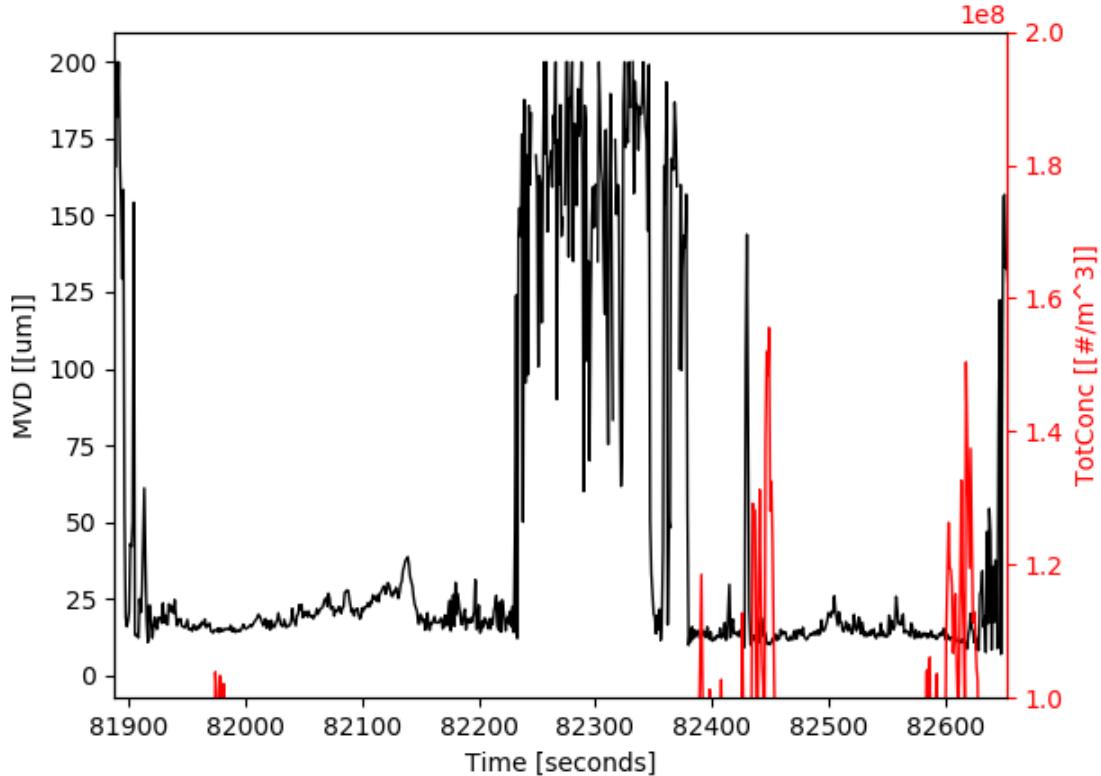


Figure 31: Mean volume diameter (black) and total concentration above 10^8 m^{-3} (red) from 22:45Z to 22:58Z during the 2/5/2020 flight.

The final scatterplots are those analyzing the mean volume diameter (Fig. 32). Looking at $0 \text{ } \mu\text{m} - 200 \text{ } \mu\text{m}$, $50 \text{ } \mu\text{m} - 200 \text{ } \mu\text{m}$, and $0 \text{ } \mu\text{m} - 50 \text{ } \mu\text{m}$ ranges, few patterns emerge, though the larger MVD's were exclusively below 0.1 g m^{-3} . MVD's above $150 \text{ } \mu\text{m}$ are assumed to be almost exclusively ice, as supercooled large drop environments were rare in IMPACTS 2020. Low RICE Probe SLWC values in high MVD regimes are encouraging since the RICE Probe is theoretically insensitive to ice. Low CDP LWC values in high MVD regimes are encouraging as it appears the CDP is not misreading large ice particles as liquid drops.

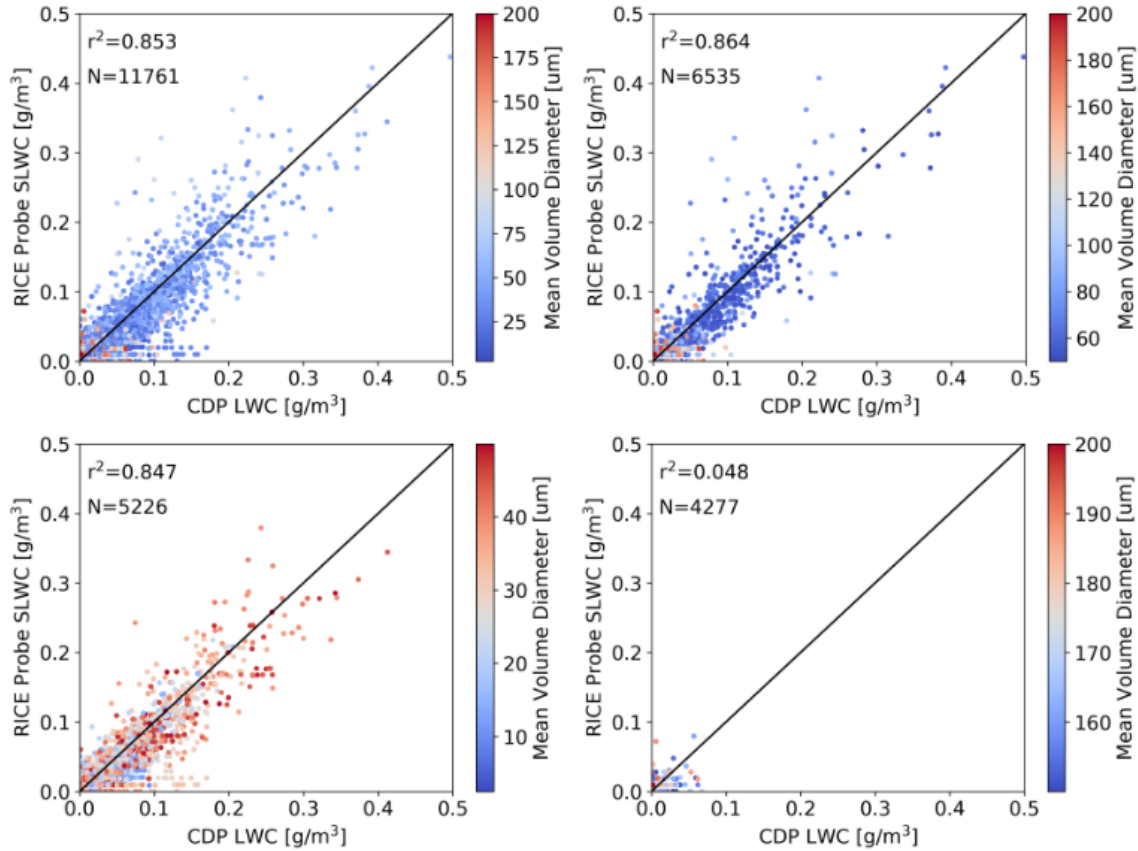


Figure 32: Scatterplots of the Rosemount Icing Detector supercooled liquid water content and Cloud Droplet Probe liquid water content. Mean volume diameter limits, from top left, clockwise: no limit, 50 μm to 200 μm , 150 μm to 200 μm , 0 μm to 50 μm .

7. Minimum Detection Threshold

Using the dt interval of 2 seconds in Eq. (5), the minimum dF/dt that can be used is 1 Hz/2 seconds. With the dimensions of the probe remaining constant throughout the lifetime of the probe and the k value having been found, the TAS is the only unknown left to determine what a minimum SLWC detection threshold is for the model 0871ND4-FT RICE Probe. This minimum threshold is inversely proportional to airspeed, so to minimize the threshold, the highest TAS has to be determined. During IMPACTS 2020, the highest TAS was 208.5 m s^{-1} during the 2/25/2020 flight. Using that value of TAS in Eq. (5) results in a minimum

detection threshold for the 0871ND4-FT model RICE Probe of 0.007 g m^{-3} , within an order of magnitude of the Heymsfield and Miloshevich (1989) value of 0.002 g m^{-3} . However, the average TAS of the 2/25/2020 flight was 139.2 m s^{-1} , resulting in an average minimum detection threshold of 0.021 g m^{-3} . While this is a higher minimum detection than in past studies, the RICE Probe should still be able to reliably measure SLWC in the 0.02 to 0.1 g m^{-3} range.

CHAPTER 5

DISCUSSION AND CONCLUSIONS

1. Discussion

Given the importance of quality measurements of supercooled liquid water to NASA's field campaign, every available tool to aid in the understanding of supercooled water should be used. Even when all traditionally available LWC probes are operational, the model 0871ND4-FT of the RICE Probe can serve a valuable role in modern field campaigns. Under proper operating conditions, the RICE Probe correlates well with the CDP LWC, and in certain circumstances could perform better than other LWC measuring probes since it is not subject to the same operational limitations or biases. The RICE Probe is insensitive to ice, which is not true for the King Probe and CDP. The RICE Probe is not subject to coincidence error or is limited to particles under 50 μm like the CDP. Unlike the King Probe, the RICE Probe is not subject to a drifting baseline and does not require zeroing in out of cloud conditions after a long period of in cloud conditions.

Because the SLWC product is derived from the CDP LWC product, the uncertainty of the product is dependent on the uncertainty of both the CDP and RICE Probe measurements. One source of uncertainty for the CDP is the uncertainty within Mie theory, because the relationship between droplet size and scattered radiation is non-monotonic, leading to uncertainty in particle sizing.

Because of a gradient in the laser intensity within the CDP sample area and the different light-scattering angles for particles with different positions, the particle size spectrum is artificially broadened, increasing the uncertainty. While there are processing methods to mitigate the effect of coincidence, it is uncertain whether it can be completely accounted for with the CDP. Uncertainty still remains with ice particle shattering in the CDP even with the presence of anti-shattering tips and processing methods that filter particles by their interarrival times. Uncertainty in the TAS calculation also impacts the CDP uncertainty because the TAS is important for the sample volume calculation, influencing the concentration and LWC calculations. These uncertainties result in a CDP LWC bias on the order of 33% (Lance et al. 2010).

The RICE Probe is not without its drawbacks or uncertainties, though the magnitude is not well documented. For all the advantages that the RICE Probe has, it can only function properly in sufficiently supercooled environments, and the digital RICE Probe is limited to a lower resolution than its LWC-measuring counterparts. Also related to the resolution is that noise in the RICE Probe signal can cause an artificial fluctuation in the data on the same order as the minimum detection threshold. There is some uncertainty regarding the treatment of the collection efficiency, which is often assumed to be unity but that assumption has not been proven to be true. Additionally, while well-documented open source software exists for the quantitative measurements from the King Probe and CDP, comparable development for the RICE Probe has not kept pace. Thus, further research for matters such as direct calculation of the Ludlam limit and other calibration techniques besides comparison with a CDP are needed.

Field campaigns such as NASA IMPACTS are prone to unavoidable instrument failure, and even with the presence of probes such as the King Probe and CDP that can fill similar roles, having maximum possible redundancy only

helps the field campaign. The CDP and King Probe were offline for the final five flights of the P-3 in 2020. Here, the RICE Probe could fill that LWC data gap, at least for when the flight legs were sufficiently below freezing. The RICE Probe was operational during that time, and using the RICE Probe-derived SLWC product could give valuable insight when in situ cloud probes were unavailable.

The analysis is valid for the model 0871ND4-FT used during the NASA IMPACTS campaign. The use of the precise derived k value for this particular probe is not recommended for use for other RICE Probes, but the derivation process is sound. While at least one study claims that the repeatability between two different RICE Probes is good (Jackson et al. 2003), multiple other sources show significant enough differences between RICE Probes to warrant separate calibrations (Baumgardner and Rodi 1989; Heymsfield and Miloshevich 1989; Mazin et al. 2001).

Caution is advised when using the RICE Probe on a different aircraft. For example, a different mounting position could cause different pitch or roll angles to “shadow” the RICE Probe and cause SLWC underrepresentation. If the probe was mounted on an aircraft operating at a higher TAS, the temperature filter would have to be adjusted to colder temperatures, the TAS effect would need to be reevaluated, and the minimum detection threshold would need to be recalculated. Also, this study did not analyze the RICE Probe response to supercooled large drops, where probe performance may be degraded by changes in factors such as collection efficiency of the cylinder and ability to completely clean the cylinder in high LWC conditions.

2. Conclusions

The Rosemount Icing Detector model 0871ND4-FT has been evaluated for its quantitative capabilities in measuring supercooled liquid water content. A SLWC

product is derived by comparing the change in the RICE Probe frequency to known LWC measurements during supercooled water-only cases and the empirical k constant in Eq. (4) was found to be $4. \times 10^{-4}$. The SLWC product is applied to the four IMPACTS 2020 flights with reliable CDP LWC data and RICE Probe data and the following limitations of RICE Probe operation were found:

- A temperature of $-3 \text{ }^{\circ}\text{C}$ is the optimal maximum temperature limit.
- A maximum pitch angle of 3° is optimal, while no lower limit is necessary.
- At the absolute fastest TAS on the NASA P-3 during IMPACTS 2020, the minimum detection threshold is 0.007 g m^{-3} , though a more typical TAS puts the minimum detection threshold at around 0.02 g m^{-3} .

Additionally, the results from the following environmental and aircraft factors that were analyzed but no limit was established:

- No roll angle limits are necessary.
- In the range of $-5 \text{ }^{\circ}\text{C}$ to $-3 \text{ }^{\circ}\text{C}$, a lower TAS led to less spread in the data relative to higher TAS, but a optimal TAS/optimal temperature relation to provide a limit on TAS is not provided.
- While IMPACTS 2020 data suggests that the RICE Probe may undersample relative to the CDP in high particle concentrations, the sample size is too small to confidently place any limits.
- Mean Volume Diameter tests show promising results that both the CDP and RICE Probe were largely not sensitive to large ice particles.

The RICE Probe has utility as a quantitative probe in addition to its current usage as a qualitative probe. As mounted on the NASA P-3, the SLWC product is a valid product for the NASA IMPACTS field campaign at temperatures at or colder than $-3 \text{ }^{\circ}\text{C}$ and at pitch angles less than 3° . The addition of the RICE

Probe's SLWC product will directly contribute to the NASA IMPACTS goal of understanding banded structures within snowstorms at the microphysical level as the only probe in the campaign that strictly measures supercooled water only. As the NASA P-3 has been utilized in many NASA Earth Science missions before and will continue to do so for the foreseeable future, the RICE Probe will continue to be trusted in the microphysical suite of instruments going forward. As long as care is taken with mounting position and being cognizant of TAS effects on the data, the methodology to derive a SLWC product from the RICE Probe can be applied to virtually any in situ mission in icing conditions, regardless of aircraft.

REFERENCES

- Bain, M., and J. F. Gayet, 1982: Aircraft Measurements of Icing in Supercooled and Water Droplet/Ice Crystal Clouds. *J. Appl. Meteorol. Climatol.*, **21**, 631–641, [https://doi.org/10.1175/1520-0450\(1982\)021<0631:AMOIIS>2.0.CO;2](https://doi.org/10.1175/1520-0450(1982)021<0631:AMOIIS>2.0.CO;2).
- Baumgardner, D., and A. Rodi, 1989: Laboratory and Wind Tunnel Evaluations of the Rosemount Icing Detector. *J. Atmospheric Ocean. Technol.*, **6**, 971–979, [https://doi.org/10.1175/1520-0426\(1989\)006<0971:LAWTEO>2.0.CO;2](https://doi.org/10.1175/1520-0426(1989)006<0971:LAWTEO>2.0.CO;2).
- Bernstein, B. C., R. M. Rasmussen, F. McDonough, and C. Wolff, 2019: Keys to Differentiating between Small- and Large-Drop Icing Conditions in Continental Clouds. *J. Appl. Meteorol. Climatol.*, **58**, 1931–1953, <https://doi.org/10.1175/JAMC-D-18-0038.1>.
- Biter, C. J., J. E. Dye, D. Huffman, and W. D. King, 1987: The Drop-Size Response of the CSIRO Liquid Water Probe. *J. Atmospheric Ocean. Technol.*, **4**, 359–367, [https://doi.org/10.1175/1520-0426\(1987\)004<0359:TDSROT>2.0.CO;2](https://doi.org/10.1175/1520-0426(1987)004<0359:TDSROT>2.0.CO;2).
- Borque, P., K. J. Harnos, S. W. Nesbitt, and G. M. McFarquhar, 2019: Improved Parameterization of Ice Particle Size Distributions Using Uncorrelated Mass Spectrum Parameters: Results from GCPEX. *J. Appl. Meteorol. Climatol.*, **58**, 1657–1676, <https://doi.org/10.1175/JAMC-D-18-0203.1>.
- Boyne, W.J., 2014: P-3 Orion. *Air Force Mag.*, **97**, 88-.
- Brown, E. N., 1981: *An Evaluation of the Rosemount Ice Detector for Aircraft Hazard Warning and for Undercooled Cloud Water Content Measurements*. UCAR/NCAR,.
- Claffey, K. J., K. F. Jones, and C. C. Ryerson, 1995: Use and calibration of Rosemount ice detectors for meteorological research. *Atmospheric Res.*, **36**, 277–286, [https://doi.org/10.1016/0169-8095\(94\)00042-C](https://doi.org/10.1016/0169-8095(94)00042-C).

- Cober, S., and G. Isaac, 2006: Estimating Maximum Aircraft Icing Environments Using a Large Database of In-Situ Observations. *44th AIAA Aerospace Sciences Meeting and Exhibit, Aerospace Sciences Meetings*, American Institute of Aeronautics and Astronautics.
- , A. Korolev, and G. Isaac, 2001a: Assessing characteristics of the Rosemount Icing Detector under natural icing conditions. *39th Aerospace Sciences Meeting and Exhibit, Aerospace Sciences Meetings*, American Institute of Aeronautics and Astronautics.
- Cober, S. G., G. A. Isaac, and A. V. Korolev, 2001b: Assessing the Rosemount Icing Detector with In Situ Measurements. *J. Atmospheric Ocean. Technol.*, **18**, 515–528, [https://doi.org/10.1175/1520-0426\(2001\)018<0515:ATRIDW>2.0.CO;2](https://doi.org/10.1175/1520-0426(2001)018<0515:ATRIDW>2.0.CO;2).
- , ———, and J. W. Strapp, 2001c: Characterizations of Aircraft Icing Environments that Include Supercooled Large Drops. *J. Appl. Meteorol. Climatol.*, **40**, 1984–2002, [https://doi.org/10.1175/1520-0450\(2001\)040<1984:COAIET>2.0.CO;2](https://doi.org/10.1175/1520-0450(2001)040<1984:COAIET>2.0.CO;2).
- Cropper, M., 2021: P-3 Orion - WFF | NASA Airborne Science Program. https://airbornescience.nasa.gov/aircraft/P-3_Orion_-_WFF (Accessed June 28, 2021).
- Delene, D., K. Hibert, M. Poellot, and N. Brackin, 2019: *The North Dakota Citation Research Aircraft Measurement Platform*. SAE International,.
- , A. Skow, J. O’Brien, N. Gapp, S. Wagner, K. Hibert, K. Sand, and G. Sova, 2020: *Airborne Data Processing and Analysis Software Package*. Zenodo,.
- Delene, D. J., 2011: Airborne data processing and analysis software package. *Earth Sci. Inform.*, **4**, 29–44, <https://doi.org/10.1007/s12145-010-0061-4>.
- Fraser, D., C. K. Rush, and D. Baxter, 1953: Thermodynamic Limitations of Ice Accretion Instruments. *Bull. Am. Meteorol. Soc.*, **34**, 146–154, <https://doi.org/10.1175/1520-0477-34.4.146>.
- Heymsfield, A., M. Krämer, N. B. Wood, A. Gettelman, P. R. Field, and G. Liu, 2017: Dependence of the Ice Water Content and Snowfall Rate on Temperature, Globally: Comparison of in Situ Observations, Satellite Active Remote Sensing Retrievals, and Global Climate Model Simulations. *J. Appl. Meteorol. Climatol.*, **56**, 189–215, <https://doi.org/10.1175/JAMC-D-16-0230.1>.

- Heymsfield, A. J., and L. M. Miloshevich, 1989: Evaluation of Liquid Water Measuring Instruments in Cold Clouds Sampled during FIRE. *J. Atmospheric Ocean. Technol.*, **6**, 378–388, [https://doi.org/10.1175/1520-0426\(1989\)006<0378:EOLWMI>2.0.CO;2](https://doi.org/10.1175/1520-0426(1989)006<0378:EOLWMI>2.0.CO;2).
- , and ———, 1993: Homogeneous Ice Nucleation and Supercooled Liquid Water in Orographic Wave Clouds. *J. Atmospheric Sci.*, **50**, 2335–2353, [https://doi.org/10.1175/1520-0469\(1993\)050<2335:HINASL>2.0.CO;2](https://doi.org/10.1175/1520-0469(1993)050<2335:HINASL>2.0.CO;2).
- Isaac, G., S. G. Cober, J. W. Strapp, A. Korolev, A. Tremblay, and D. L. Marcotte, 2001: Recent Canadian Research on Aircraft In-Flight Icing. *Can. Aeronaut. Space J.*, **44**, 213–222.
- Jackson, D., D. Cronin, J. Severson, and D. Owens, 2001a: Ludlam limit considerations on cylinder ice accretion - Aerodynamics and thermodynamics. *39th Aerospace Sciences Meeting and Exhibit, Aerospace Sciences Meetings*, American Institute of Aeronautics and Astronautics.
- , D. Owens, D. Cronin, and J. Severson, 2001b: Certification and integration aspects of a primary ice detection system. *39th Aerospace Sciences Meeting and Exhibit, Aerospace Sciences Meetings*, American Institute of Aeronautics and Astronautics.
- Jackson, D. G., J. Y. Liao, and J. A. Severson, 2003: An Assessment of Goodrich Ice Detector Performance in Various Icing Conditions. FAA In-flight Icing / Ground De-icing International Conference & Exhibition, 2003-01–2115.
- Jeck, R. K., 2007: Calibration and Use of Goodrich Model 0871FA Ice Detectors in Icing Wind Tunnels. *J. Aircr.*, **44**, 300–309, <https://doi.org/10.2514/1.23543>.
- King, W. D., D. A. Parkin, and R. J. Handsworth, 1978: A Hot-Wire Liquid Water Device Having Fully Calculable Response Characteristics. *J. Appl. Meteorol. Climatol.*, **17**, 1809–1813, [https://doi.org/10.1175/1520-0450\(1978\)017<1809:AHWLWD>2.0.CO;2](https://doi.org/10.1175/1520-0450(1978)017<1809:AHWLWD>2.0.CO;2).
- Korolev, A., 2007: Limitations of the Wegener–Bergeron–Findeisen Mechanism in the Evolution of Mixed-Phase Clouds. *J. Atmospheric Sci.*, **64**, 3372–3375, <https://doi.org/10.1175/JAS4035.1>.

- Korolev, A., and Coauthors, 2017: Mixed-Phase Clouds: Progress and Challenges. *Meteorol. Monogr.*, **58**, 5.1-5.50, <https://doi.org/10.1175/AMSMONOGRAPHS-D-17-0001.1>.
- Lance, S., 2012: Coincidence Errors in a Cloud Droplet Probe (CDP) and a Cloud and Aerosol Spectrometer (CAS), and the Improved Performance of a Modified CDP. *J. Atmospheric Ocean. Technol.*, **29**, 1532–1541, <https://doi.org/10.1175/JTECH-D-11-00208.1>.
- Lance, S., C. A. Brock, D. Rogers, and J. A. Gordon, 2010: Water droplet calibration of the Cloud Droplet Probe (CDP) and in-flight performance in liquid, ice and mixed-phase clouds during ARCPAC. *Atmospheric Meas. Tech.*, **3**, 1683–1706, <https://doi.org/10.5194/amt-3-1683-2010>.
- Mazin, I. P., A. V. Korolev, A. Heymsfield, G. A. Isaac, and S. G. Cober, 2001: Thermodynamics of Icing Cylinder for Measurements of Liquid Water Content in Supercooled Clouds. *J. Atmospheric Ocean. Technol.*, **18**, 543–558, [https://doi.org/10.1175/1520-0426\(2001\)018<0543:TOICFM>2.0.CO;2](https://doi.org/10.1175/1520-0426(2001)018<0543:TOICFM>2.0.CO;2).
- McMurdie, L. A., G. Heymsfield, J. E. Yorks, and S. A. Braun, 2020: IMPACTS Field Campaign Data Collection. <https://doi.org/10.5067/IMPACTS/DATA101>.
- Plummer, D. M., G. M. McFarquhar, R. M. Rauber, B. F. Jewett, and D. C. Leon, 2014: Structure and Statistical Analysis of the Microphysical Properties of Generating Cells in the Comma Head Region of Continental Winter Cyclones. *J. Atmospheric Sci.*, **71**, 4181–4203, <https://doi.org/10.1175/JAS-D-14-0100.1>.
- Rogers, R. R., and M. K. Yau, 1989: *A Short Course in Cloud Physics*. 3rd ed. Elsevier, 290 pp.
- Storelvmo, T., and I. Tan, 2015: The Wegener-Bergeron-Findeisen process – Its discovery and vital importance for weather and climate. *Meteorol. Z.*, 455–461, <https://doi.org/10.1127/metz/2015/0626>.
- Strapp, J., P. Chow, M. Maltby, A. Bezer, A. Korolev, I. Stromberg, and J. Hallett, 1999: Cloud microphysical measurements in thunderstorm outflow regions during Allied/BAE 1997 flight trials. *37th Aerospace Sciences Meeting and Exhibit*, 498.

Stull, R. B., 2000: *Meteorology for Scientists and Engineers*. 2nd ed. Gary
Garlson, 502 pp.

Twohy, C. H., and D. Rogers, 1993: Airflow and Water-Drop Trajectories at
Instrument Sampling Points around the Beechcraft King Air and Lockheed
Electra. *J. Atmospheric Ocean. Technol.*, **10**, 566–578,
[https://doi.org/10.1175/1520-0426\(1993\)010<0566:AAWDTA>2.0.CO;2](https://doi.org/10.1175/1520-0426(1993)010<0566:AAWDTA>2.0.CO;2).

APPENDIX A

SCRIPTS

Beyond the scripts in ADPAA, some Python 3 scripts were developed that were useful in this study. The code “2DS_GT100_v2.py” has no arguments, but depending on which times of given cases from the four flights between 1/25/2021 and 2/7/2021 are commented out, will make a logfile of the maximum concentration, maximum mean diameter, average mean diameter, and average concentration of the 2D-S probe horizontal distribution data. The code “Adiabatic_Compression.py”, given the arguments of the IMPACTS summary file and the start and end time in seconds after midnight UTC will generate two plots. One plot is a time plot of the air temperature and the adiabatic surface temperature as calculated by Mazin et al. (2001). The other plot is the difference between the air temperature and the adiabatic surface temperature, such as in Figure 3. The code “RICE_Case_Comp.py” has no arguments, but reads the 2/5/2020 IMPACTS summary file and generates scatterplots of RICE Probe $-(dF/dt)/TAS$ for a cold SLWC case (Figure 8) and a warm case (Figure 9). The code “RICE_CDP_NoErr.py”, given the arguments of the IMPACTS summary file and the start and end time in seconds after midnight UTC, will generate a time plot of CDP and King Probe LWC and RICE Probe Frequency, such as in Figure 5, Figure 6, and Figure 10. The code “RICE_Combined_Test.py” is the main code for the scatterplots throughout the thesis. This code takes no arguments, but a block of code near the top of the program can be adjusted to make plots of RICE Probe vs CDP, RICE Probe vs King Probe, CDP vs King Probe, or all three, and

has adjustable boundaries for temperature, pitch angle, roll angle, TAS, concentration, and MVD, plus the variable that is color coded can be changed as well. This code, along with some supplemental data is available via SourceForge at <https://sourceforge.net/projects/greg-sova-master-thesis/> .